architecture

MDPI

Article

Nature-Based Solutions for Urban Microclimate Resilience in Hot Arid Regions

Ameena El Zeiny [1,*], Samah El Khateeb [2,3] and Wesam M. El-Bardisy [1]

[1] Department of Urban Design and Planning, Faculty of Engineering, Ain Shams University, Cairo 11517, Egypt; welbardisy@eng.asu.edu.eg
[2] Architectural Engineering Department, University of Business and Technology, Jeddah 21448, Saudi Arabia; samah.elkhateeb@eng.asu.edu.eg
[3] Smart and Future Cities Laboratory for Sustainable Urban Solutions, Faculty of Engineering, Ain Shams University, Cairo 11517, Egypt
* Correspondence: ameenaelzeiny@gmail.com; Tel.: +20-1091311101 or +971-504756862

Abstract

Urban areas in hot-arid regions face extreme temperatures, water scarcity, and deteriorating air quality, intensified by rapid urbanization and climate change. In the Greater Cairo Region, road-network redevelopment has reduced street greenery, increasing the need for strategies that compensate for lost shade, cooling, and ecosystem services. This study evaluates nature-based solution (NBS) configurations in a road-widened street corridor in Zahraa El Maadi, Cairo, Egypt. Seven ENVI-met 5.9.0 scenarios, varying in tree-canopy, grass, green-roof, and water coverage, were compared over a 24 h peak-summer period. Air temperature (Ta), wind speed (WS), relative humidity (RH), and physiological equivalent temperature (PET) were assessed at three pedestrian-level receptors at 12:00, 16:00, and 20:00, and i-Tree MyTree was used to estimate complementary carbon, runoff, and air-quality co-benefits for a representative *Ficus microcarpa* tree. Scenarios with greater tree-canopy cover generally produced lower pedestrian-level Ta, with reductions of approximately 0.4–1.6 °C depending on receptor location and time of day. A one-at-a-time sensitivity analysis of air-temperature forcing (±2 °C) and inflow wind speed (3.0 and 6.0 m/s) showed that the higher-tree-canopy scenario was cooler than the no-vegetation reference in only 21 of 36 comparisons, so its advantage depended on forcing condition, location, and time. The maximum-NBS scenario was not consistently the best performer, highlighting the influence of urban morphology and NBS placement. Water features increased RH but did not consistently reduce PET, while green roofs and grass provided limited direct pedestrian-level benefits. Overall, NBS reduced but did not eliminate heat stress. The study proposes a decision matrix that links site assets, microclimate simulation, ecosystem-service assessment, and water demand, including greywater reuse and efficient irrigation, to support NBS planning in hot-arid urban redevelopment.

Keywords: nature-based solutions; urban microclimate; green infrastructure; hot-arid regions; urban heat island; climate resilience and adaptation; ENVI-met simulation

Academic Editor: Zhonghua Gou

Received: 17 August 2026
Revised: 13 October 2026
Accepted: 23 October 2026
Published: 30 October 2026

Copyright: © 2026 by the authors. Licensee MDPI, Basel, Switzerland. This article is an open access article distributed under the terms and conditions of the Creative Commons Attribution (CC BY) license.

1. Introduction

With increasing population density and urbanization rates, extreme weather events have become more frequent, leading to numerous negative environmental effects [1]. According to climate projections, cities are expected to face greater effects of climate change

due to ecosystem destruction, lack of vegetation, densification of built-up areas, and the resulting prevalence of impermeable surfaces [1]. The impact of climate change has attracted the attention of numerous urban planners due to the recognized rise in atmospheric temperatures in urban areas, especially in hot-arid climatic zones [2]. Hot-arid cities are especially vulnerable to the urban heat island (UHI) phenomenon because high solar exposure, elevated carbon dioxide concentrations compared with surrounding rural areas, extensive impervious surfaces, low vegetation coverage, and water scarcity interact with dense development and transport infrastructure [2]. These conditions increase heat storage and pedestrian exposure, making the spatial distribution of shade and evapotranspiration a central concern for urban planning and design [3,4].

Accordingly, many cities are implementing, researching, and piloting nature-based solutions (NBSs), which incorporate nature and related ecosystem services, as an alternative to grey or technology-based infrastructure to respond to these challenges. The most widely used NBS definitions are those of the International Union for Conservation of Nature (IUCN) and the European Commission. The IUCN defines NBSs as actions to protect, sustainably manage, and restore natural or modified ecosystems that address societal challenges effectively and adaptively, simultaneously providing human well-being and biodiversity benefits. The European Commission, in turn, defines NBSs as actions that are inspired by, supported by, or copied from nature, which aim to help societies address a variety of environmental, social, and economic challenges in sustainable ways [5]. These two definitions share the same understanding of NBSs as actions taken to address societal challenges through ecosystem processes [6]. NBSs vary in effectiveness depending on the scale at which they are implemented. At the street scale, trees can reduce radiant exposure through direct shade and support evaporative cooling. Grass, green roofs, and water surfaces operate through different mechanisms and at different heights, so their benefits at the pedestrian level are not necessarily equivalent [7]. NBSs can provide sustainable, resilient, cost-effective, and multifunctional solutions to many problems related to sustainable urban development [8].

With a focus on hot-arid regions, scholars have actively investigated NBSs and their impacts on urban environments since 2008 [9]. A systematic review by Meerow et al. [10] found that NBSs can reduce air temperature by up to 7 °C depending on the vegetation type, its physical characteristics, and its spatial distribution. Soltanifard and Amani-Beni [11] highlighted that during peak summer periods, green infrastructure provides greater temperature reductions and lower building cooling loads than blue infrastructure. Furthermore, Elnabawi et al. [12] noted that NBS implementation, depending on contextual conditions and urban morphology, can substantially mitigate urban heat-island effects, runoff, and air pollution.

Although the integration of NBS in hot-arid regions offers benefits, it also faces various challenges that may hinder its application and implementation in this context [13]. These challenges include extreme heat and water scarcity, which may directly affect plant survival and lead to high maintenance costs. In terms of governance, there are significant gaps: limited knowledge of NBS implementation, a strong reliance on grey infrastructure, and a focus on short-term actions driven by financial constraints rather than on long-term NBS strategies. Moreover, comprehensive implementation guidelines and performance-evaluation metrics that integrate NBSs into a cohesive framework linked to urban development pathways are still lacking, especially in developing and arid contexts.

Egypt, especially the Greater Cairo Region, is currently undergoing redevelopment of its urban vehicular network, which is expected to alter the local microclimate because part of the green fabric has been removed from certain streets. Cairo, known for its hot and dry climate, is being affected by rising temperatures and increasing greenhouse gas emissions due to rapid population growth, expanding road networks, and increased land use [14]. These pressures are expected to escalate, influencing not only the city's environmental performance but also the functionality of public spaces, infrastructure efficiency, and overall urban livability [15]. In Zahraa El Maadi, for example, the roadway was widened, and the central green island was reduced, creating a practical need to test compensatory interventions within the remaining street geometry.

Thus, a clear research gap remains: the literature and case studies on NBSs predominantly emphasize their effects while giving limited attention to their integration into urban development, particularly in mobility-led redevelopment, where the loss of pedestrian shade and ecosystem services is often treated as a secondary effect. This presents a significant opportunity to incorporate NBSs tailored to specific hot-arid contexts. This paper therefore addresses two research questions: (1) How, and to what extent, can NBS contribute to transformational change in space-limited urban development in arid regions? (2) What performance-evaluation metrics could support decisions on implementing NBSs in arid regions?

To address these questions, this study aims to identify feasible combinations of NBSs (trees, grass, green roofs, and water surfaces) that provide the most beneficial pedestrian-scale microclimatic response in transport-led redevelopment, using the case study of Zahraa El Maadi Street, and to translate simulation outputs into urban-planning priorities. The objectives are to (1) compare the microclimatic performance of seven NBS scenarios; (2) explain the mechanisms and spatial differences behind scenario performance; (3) connect the tree-based scenario results with complementary ecosystem-service estimates from i-Tree; and (4) develop a quantitative decision matrix for hot-arid street redevelopment that links post-development site conditions to water demand, microclimate simulation, and tree ecosystem-service potential.

Accordingly, the contribution of this study lies not in demonstrating the general cooling effect of urban vegetation, which is already well established, but in linking mobility-led green-space loss with site-specific NBS scenario assessment and translating the resulting microclimatic and ecosystem-service evidence into an integrated planning framework for hot-arid urban redevelopment.

2. Materials and Methods

To achieve these objectives, comparative numerical modeling using ENVI-met was conducted to examine how alternative NBS configurations influence the pedestrian-level microclimate of a road-widened street corridor in a hot-arid urban context. The workflow comprised five main steps: (1) defining the study area and collecting spatial and climatic data; (2) constructing the ENVI-met simulation models; (3) running the simulations and analyzing the resulting microclimatic outputs; (4) evaluating thermal-comfort conditions using BIO-met and LEONARDO; and (5) assessing the ecosystem-service performance of the selected tree using i-Tree, including carbon sequestration and related co-benefits. The scenario results, together with the literature and current development plans, were then synthesized into an integrated planning framework for NBS implementation (see Figure 1).

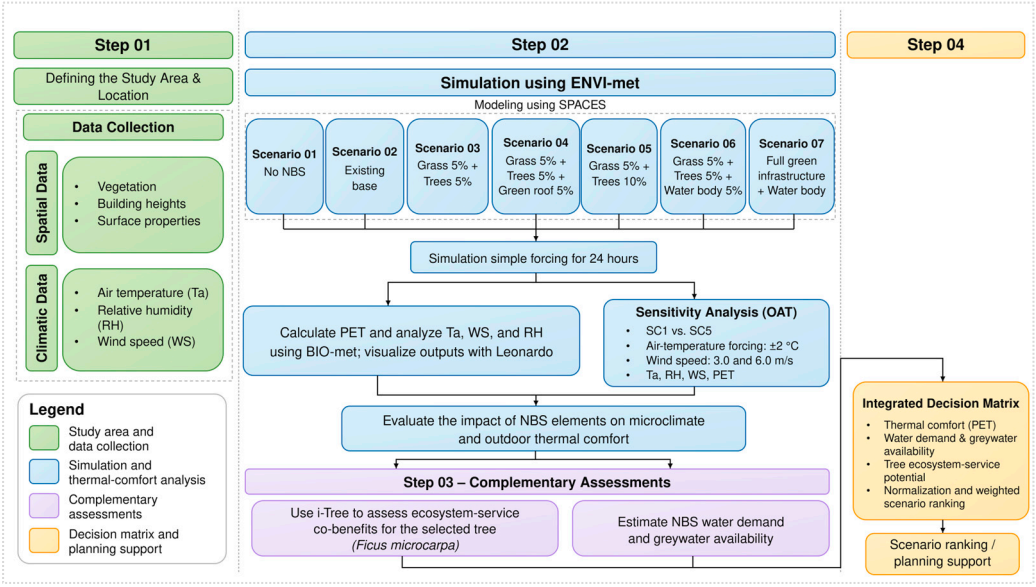


Figure 1. Research workflow.

2.1. Study Area and Planning Context

El Maadi, a green suburban district south of central Cairo, Egypt, was selected as the case-study context (see Figure 2). It is one of Cairo's well-known residential districts and is characterized by extensive green spaces, tree-lined streets, and a relatively peaceful, pedestrian-friendly environment. These open green spaces contribute significantly to Maadi's distinctive urban character and environmental quality compared with many denser parts of Cairo.

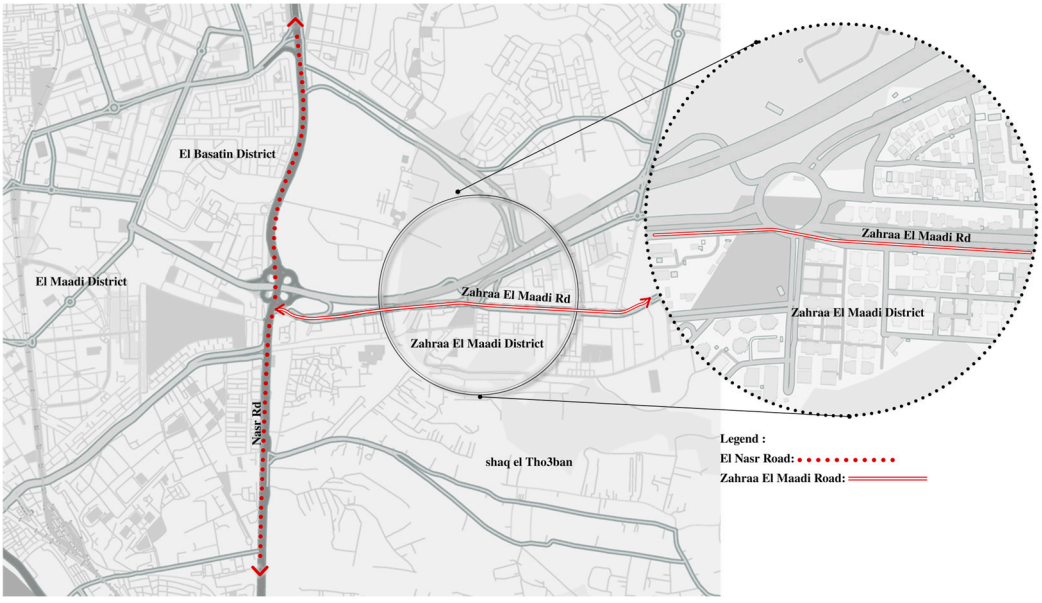


Figure 2. Location of the study area.

The study area lies along Zahraa El Maadi Street, at latitude 29°57′42.51″ N and longitude 31°18′14.32″ E. The street is oriented west–east. Beyond its relevance to mobility-led urban redevelopment, Zahraa El Maadi was selected because of its proximity to Shaq El Tho'ban, one of the largest marble and granite industrial zones in the region and a major source of air pollution. According to the IQAir index, air quality in the study area is categorized as "unhealthy for sensitive groups" owing to continuous dust and particulate emissions from stone-cutting and processing operations, which can also contaminate water and soil and affect public health in the surrounding urban areas [16].

2.2. Urban Character and Road-Widening Change

In 2025, Zahraa El Maadi Street underwent a mobility-oriented redevelopment that altered both the street geometry and land-cover composition. The asphalt roadway was widened from approximately 10 m to 14 m, representing a 40% increase in roadway width. At the same time, the central green island was reduced from approximately 17 m to 9 m, corresponding to an approximately 47% reduction in its width. In terms of the total street-area composition shown in Figure 3, the road-surface area increased from approximately 25% to 30%, representing an increase of 5 percentage points, while the green-space surface area decreased from approximately 20% to 5%, representing a reduction of 15 percentage points. Part of the former green area was also converted into a sand-surfaced roundabout. These existing site conditions were used as the physical basis for constructing the baseline ENVI-met model and for defining the subsequent NBS scenarios.

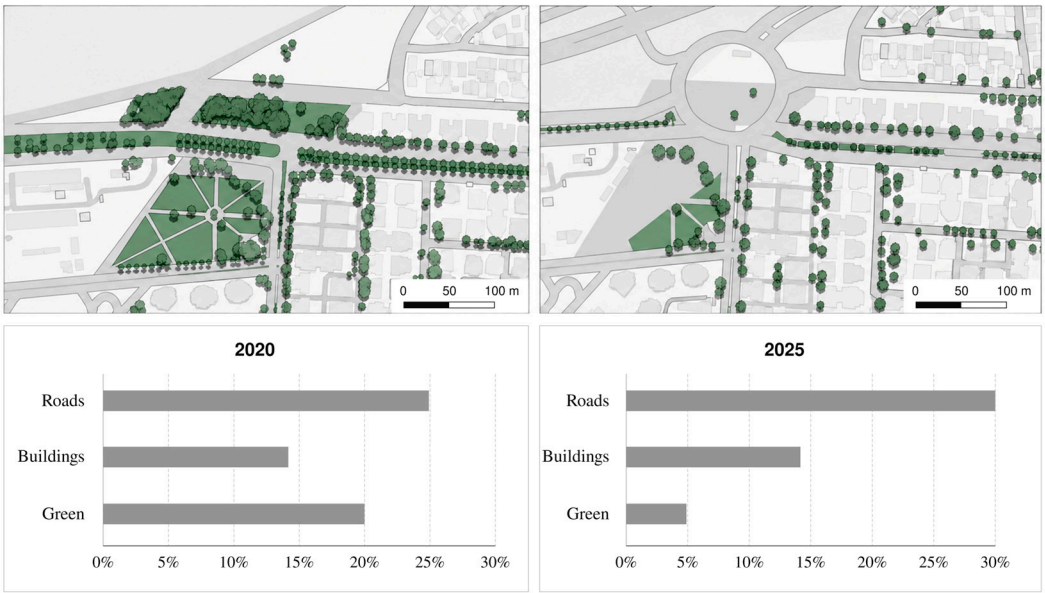


Figure 3. Comparison of street-area composition before and after redevelopment (percentage of total study-area surface).

Most buildings are mid-rise residential blocks of four to five floors. The total length of the street is 620 m. The street section in Figure 4 illustrates the current surface materials (asphalt, green, and concrete surfaces) of the redeveloped street. The green area in the middle of the street covers approximately 6527 m^2, accounting for 5% of the total street area. The existing trees and palms cover approximately 2% of the total area and are located within the central green island and along the sidewalks adjacent to the buildings (Figure 5).

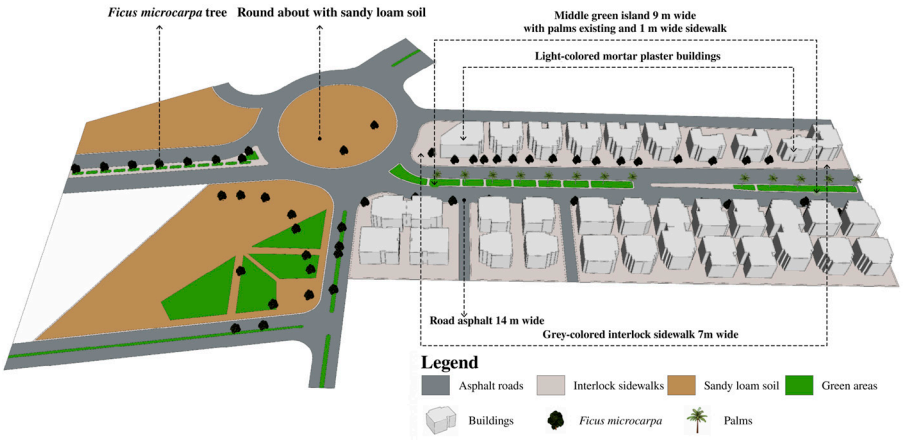


Figure 4. Current street section and surface configuration after redevelopment.



https://doi.org/10.3390/architecture6040201

Figure 5. Current conditions of the Zahraa El Maadi study corridor, showing the widened roadway, reduced central green island, existing vegetation, and surrounding residential morphology (captured on 23 October 2025).

2.3. Numerical Simulation

ENVI-met was selected because it resolves interactions among buildings, vegetation, surfaces, radiation, and near-ground atmospheric conditions at the neighborhood and street scales. General computational fluid dynamics (CFD) tools provide detailed simulations of airflow, ventilation, and pollutant dispersion and are considered to offer highly accurate airflow modeling and flexible physics [17]. However, these tools involve complex setups, incur high computational costs, and require separate calculations for thermal comfort [18]. PALM-4U is a district- to city-scale urban climate model suitable for urban heat-island and large-scale climate simulations, but it requires substantial computational resources and is less detailed at the pedestrian scale [19]. RayMan focuses on radiation and thermal-comfort analysis using rapid calculations and is useful for shading and comfort studies, but it has limited representation of airflow and vegetation interactions [20]. SOLWEIG similarly resolves spatial variations in radiant fluxes and mean radiant temperature but does not simulate airflow [21].

ENVI-met, by contrast, is a comprehensive 3D model based on the principles of fluid and heat dynamics, specifically built to examine small-scale thermal behavior in urban settings. With a typical spatial resolution of approximately 0.5–10 m and a temporal resolution ranging from 1 to 5 s, it can simulate the interactions between buildings, vegetation, and the atmosphere [22]. This capability makes it especially useful for assessing how minor changes in urban design can influence the local microclimate [23].

Modeling with ENVI-met allows different building materials, surface types, and vegetation to be integrated to study their impact on the local microclimate and to design strategies that reduce urban heat stress. As a predictive numerical model, ENVI-met also supports the planning of future urban spaces that aim for more sustainable living conditions. The simulations generate a wide range of output data, including meteorological variables such as air temperature, wind speed, and relative humidity, as well as thermal-comfort indices such as the predicted mean vote (PMV), predicted percentage dissatisfied (PPD), physiological equivalent temperature (PET), universal thermal climate index (UTCI), and standard effective temperature (SET) [24].

The 3D models were created using the SPACES tool of the ENVI-met suite, starting with a base model representing the existing conditions of the study area. From this base, the seven scenarios were developed by modifying the NBS elements (Section 2.8). The model input data and simulation settings are summarized in Tables 1 and 2.

2.4. Microclimate and Boundary Conditions

According to the Köppen climate classification, Cairo has a hot-arid (BWh) climate. The analysis used the weather file recorded at Cairo International Airport [25]. In a typical summer week, daytime temperatures range from 38 °C to 42 °C, with a relative humidity of approximately 20%, whereas in a typical winter week, they range from 18 °C to 23 °C, with a relative humidity of approximately 45%. During intense heatwaves, temperatures can rise further, while wind speeds remain relatively steady with only slight changes throughout the year. In a typical winter week, the wind speed fluctuates from 4.0 m/s to 5.5 m/s, while in a typical summer week, the average wind speed ranges from 4.5 m/s to 6.5 m/s. The prevailing wind blows from the north, followed by the northeast and northwest. The values above describe typical daytime summer conditions in Cairo, while Table 2 summarizes the 24 h forcing used for the selected simulation day, including cooler

nighttime and early-morning conditions. Boundary conditions and simulation settings are further discussed in Section 2.6.

Table 1. Input data and initial settings for the ENVI-met model.

Model Location	**Value(s) Used**
Name of location	Zahraa El Maadi
Position	Latitude 29°57′42.51″ N Longitude 31°18′14.32″ E
Model Geometry	
Domain size	620 m × 276 m
Model dimension	X-Grids = 155 Y-Grids = 69 Z-Grids = 30
Size of grid cell	dX = 4 m dY = 4 m dZ = 1 m
Model rotation out of the grid from the north	0°
Height of 3D model top	30 m

Table 2. Settings of the ENVI-met simulation.

Simulation Setting	**Value(s) Used**
Start day	20 July 2024
Start time	07:00
Total simulation time (h)	24 h
Air temperature (°C)	Min. = 26.4 °C, Max. = 40 °C (simple forcing)
Relative humidity (%)	Min. = 27%, Max. = 59%
Wind speed (m/s)	4.5 m/s
Wind direction (°)	0 (north)
Roughness length (m)	0.01
Cloud cover	Default settings in ENVI-met
Building wall and roof materials	Default settings in ENVI-met
Soil	Sandy soil (physical properties based on the ENVI-met database)
Comparability	Building geometry and meteorology were held constant across scenarios; only the specified NBS elements were changed.

The model assumes that the represented geometry and land-cover categories are adequate for cross-scenario comparison during the selected 24 h period. Building wall and roof materials, soil properties, cloud cover, and meteorological forcing were held constant. These assumptions reduce the number of variable parameters but also limit the ability to generalize absolute values beyond the modeled day and site.

2.5. Assessed Parameters

Air temperature (Ta) is the temperature of the ambient air, typically measured at 1.5–2 m above ground; it represents the local thermal state of the atmosphere [26]. It strongly influences perceived heat stress (unit: °C) [27]. Wind speed (WS) is the horizontal speed of airflow measured at a standard height (usually 1.5–2 m); it governs convective heat transfer and ventilation in outdoor spaces (unit: m/s) [28]. Relative humidity (RH) is the amount of water vapor in the air expressed as a percentage of the saturation amount at the same temperature. It affects evaporation and thermal comfort; higher RH reduces evaporative cooling (unit: %) [4]. Physiological equivalent temperature (PET) was selected as the principal thermal-comfort index because it combines air temperature, humidity,

wind speed, and radiation-related thermal load in a single equivalent temperature expressed in degrees Celsius. This makes it interpretable for planners and allows for comparison with previous outdoor-comfort studies in Cairo and other hot-arid contexts. PET is used here as a comparative indicator among scenarios, not as a substitute for direct observation of individual thermal perception [28].

The PET classification relates physiological equivalent temperature values to thermal perception and the corresponding level of physiological stress. PET values below 18 °C indicate various degrees of cold stress, from slight cold stress to extreme cold stress; 18–23 °C is considered thermally comfortable with no thermal stress. Values of 23–29 °C indicate slightly warm conditions and slight heat stress. Values of 29–35 °C denote warm conditions and moderate heat stress. PET values of 35–41 °C are considered hot and linked to strong heat stress, and values above 41 °C indicate very hot conditions and extreme heat stress. This classification provides a clear framework for interpreting pedestrian thermal comfort and comparing heat-stress severity between scenarios and receptor locations [29].

i-Tree is a free, peer-reviewed software suite developed by the United States Department of Agriculture (USDA) Forest Service and partners. It evaluates the structure, ecosystem services, and economic value of trees and urban forests and can be applied to individual trees, neighborhoods, and entire cities. The software calculates benefits such as carbon storage, air-pollution removal, and stormwater reduction, and can also evaluate energy impacts and their economic value. Therefore, i-Tree supports evidence-based tree planting, canopy management, urban forest planning, and long-term environmental planning [30].

2.6. Simulation Settings

The simulation was conducted over a 24 h period, beginning at 07:00 on 20 July 2024 and ending at 07:00 on 21 July 2024. The selected date represents peak-summer conditions (see Figure 6) and was used to provide a controlled basis for comparing the relative microclimatic performance of the seven NBS configurations. Accordingly, the study was designed as a single-day comparative assessment rather than as an evaluation of prolonged heatwave behavior or cumulative thermal processes across consecutive days. Meteonorm, which uses global climate data (e.g., temperature, precipitation, and solar radiation) to generate realistic hourly weather records exportable in formats such as EnergyPlus Weather (EPW), was used to identify this day [31]. Simple forcing was applied to define the meteorological boundary conditions (air temperature, relative humidity, wind speed, and wind direction) [25]. The results are therefore interpreted as relative differences among scenarios under the selected meteorological conditions and are not intended to represent multi-day heatwave dynamics or cumulative thermal carry-over.

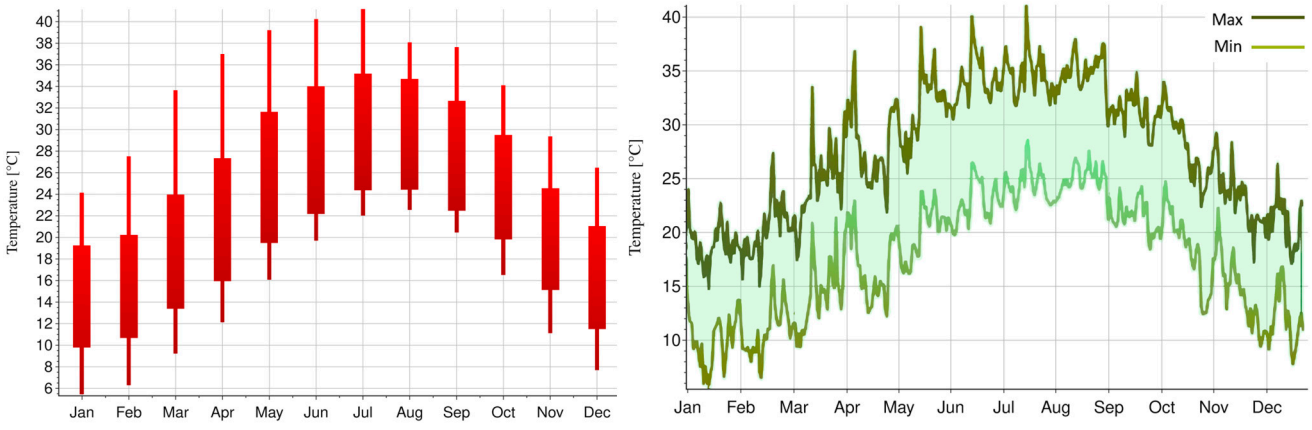


Figure 6. Monthly (**left**) and daily (**right**) temperature data used to select the simulation period, generated using Meteonorm and visualized using Ecotect.

The simulation started at 07:00; ENVI-met recommends initialization at night or near sunrise, and sufficient model spin-up before simulation outputs are interpreted [25]. The reporting times of 12:00, 16:00, and 20:00 correspond to 5, 9, and 13 h after initialization, respectively. Because the 12:00 output occurs earlier in the simulation, it is interpreted with greater caution than the later outputs. All scenarios were initialized using identical soil, surface, and atmospheric conditions; therefore, initialization effects are expected to influence absolute values more strongly than the relative differences among scenarios. Comparable single-day ENVI-met approaches have been used for comparative greening assessments in hot-arid environments; for example, Benlahbib et al. [28] simulated a single 24 h extreme summer day, while Gomaa et al. [32] used 24 h forcing to compare vegetation scenarios.

2.7. Model Reliability and Contextual Validation Evidence

ENVI-met has been widely applied in urban microclimate studies, including in hot-arid environments [14,33]. However, site-specific field validation of the present Zahraa El Maadi model was not possible because of site-security constraints and limited availability of measurement equipment. Therefore, the current model was not directly validated against on-site measurements.

A previous Cairo study [14] is cited only as contextual evidence of ENVI-met performance under comparable climatic conditions. In that study, the coefficient of determination (R^2) and index of agreement (IA) values were 0.8946 and 0.50 for air temperature, 0.971 and 0.839 for relative humidity, and $R^2 = 0.6957$ for wind speed. The moderate IA for air temperature (0.50), despite a high R^2, indicates that the earlier model reproduced the temporal pattern of air temperature more closely than its absolute values. These results do not constitute validation of the present model configuration. Accordingly, absolute simulated values remain subject to uncertainty. Because all seven scenarios were simulated using identical building geometry, meteorological forcing, materials, and model settings, the controlled setup provides a consistent basis for interpreting relative scenario-to-scenario differences, although it does not eliminate uncertainty in the absolute simulated values.

Additional contextual evidence is provided by the hot-arid ENVI-met validation and sensitivity study of Ayyad and Sharples [33]. Their analysis examined variations in wind speed, relative humidity, albedo, and grid size and reported stronger agreement for air temperature and wind speed than for relative humidity. This evidence reinforces the need for cautious interpretation of RH-based results. To address uncertainty in the present model directly, a targeted one-at-a-time (OAT) sensitivity analysis was conducted for SC1 and SC5 by perturbing air-temperature forcing by ±2 °C and changing the inflow wind speed from the 4.5 m/s baseline to 3.0 m/s and 6.0 m/s. Details are provided in Section Sensitivity Analysis.

The cited Cairo studies provide contextual evidence regarding ENVI-met performance under comparable climatic conditions but do not constitute direct validation of the present Zahraa El Maadi model. Accordingly, the results of this study are interpreted primarily as relative differences among scenarios simulated under identical model settings, while absolute values remain subject to uncertainty.

Sensitivity Analysis

A targeted one-at-a-time (OAT) sensitivity analysis was conducted to examine the dependence of the relative microclimatic response of SC1 and SC5 on selected meteorological boundary conditions. SC1 represents the reference condition without vegetation, whereas SC5 represents the higher-tree-canopy configuration (10% tree-canopy cover and 5% grass; Section 2.8). Air-temperature forcing and inflow wind speed were selected because they directly influence pedestrian-level thermal conditions and airflow.

The baseline air-temperature forcing of 26.4–40.0 °C was perturbed by ±2 °C, producing low-temperature forcing of 24.4–38.0 °C and high-temperature forcing of 28.4–42.0 °C. The baseline inflow wind speed of 4.5 m/s was changed to 3.0 m/s and 6.0 m/s for the low- and high-wind conditions, respectively. Following the OAT approach, only one meteorological parameter was modified at a time, while model geometry, land cover, materials, wind direction, relative-humidity forcing, and all other simulation settings were held constant (Table 3).

Table 3. Input conditions for the OAT sensitivity analysis.

Condition	Air-Temperature Forcing	Wind Speed	Scenarios
Baseline	26.4–40.0 °C	4.5 m/s	SC1, SC5
Low temperature	24.4–38.0 °C	4.5 m/s	SC1, SC5
High temperature	28.4–42.0 °C	4.5 m/s	SC1, SC5
Low wind	26.4–40.0 °C	3.0 m/s	SC1, SC5
High wind	26.4–40.0 °C	6.0 m/s	SC1, SC5

Eight additional ENVI-met simulations were performed, comprising low- and high-temperature and low- and high-wind conditions for both SC1 and SC5. Air temperature (Ta), relative humidity (RH), wind speed (WS), and physiological equivalent temperature (PET) were extracted from the ENVI-met outputs at the same three pedestrian-level receptors and reporting times (12:00, 16:00, and 20:00) used in the principal scenario analysis.

For each perturbed condition, sensitivity was quantified from the SC5–SC1 difference at the same receptor and reporting time:

$$\Delta X_i = X_{SC5,i} - X_{SC1,i}, \quad X \in \{Ta, RH, WS, PET\}$$

where i denotes each receptor–time combination. Negative ΔTa and ΔPET indicate lower Ta and PET in SC5, respectively. Negative ΔRH and ΔWS indicate lower RH and local WS in SC5, whereas positive values indicate higher values.

For each condition, the mean response across the nine receptor–time combinations was calculated as:

$$\overline{\Delta X} = \frac{1}{n}\sum_{i=1}^{n} \Delta X_i$$

where n = 9 represents three receptors × three reporting times.

The robustness of the scenario ranking used for planning decisions was examined separately in the decision matrix by varying the weighting profile (Sections 2.11 and 3.6). The sensitivity analysis was intended to assess the dependence of the relative SC1–SC5 response on meteorological forcing.

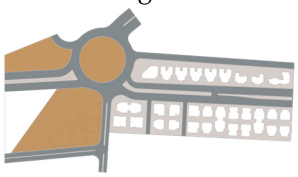
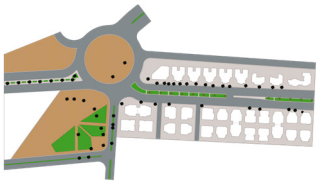
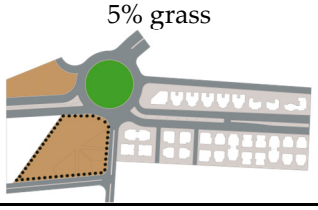
For the overall sensitivity summary, the four perturbed conditions were pooled, yielding 36 receptor–time–condition comparisons (4 conditions × 3 receptors × 3 reporting times). Results were interpreted from the overall response pattern rather than from isolated small differences.

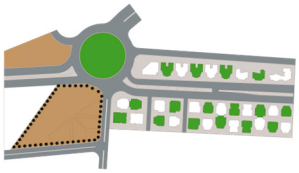
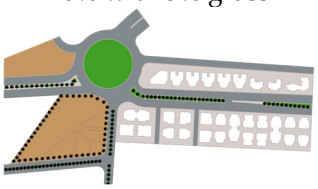
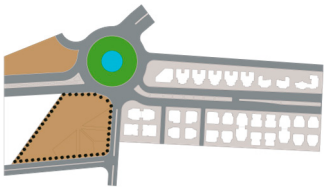
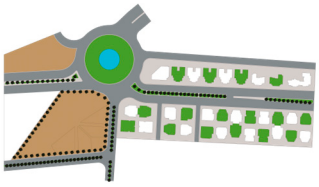
2.8. NBS Scenarios

The seven scenarios were designed as a structured comparison rather than an exhaustive optimization. The selected percentages reflect three considerations: (1) the approximate magnitude of green-space loss associated with the redevelopment; (2) the limited residual space available in the roundabout, park, central island, sidewalks, and roofs; and (3) the need to distinguish the main cooling mechanisms. Tree-canopy cover was varied to test pedestrian shading; grass was retained as a low-height permeable surface; green roofs were tested as a roof-level intervention with limited direct pedestrian shade; and water was included to test evaporative effects while recognizing the water-scarcity context. The same average tree crown size was assumed for all proposed scenarios; therefore, 5% canopy was represented by 70 trees and 10% canopy by 140 trees, while SC2 retained the observed existing condition of 54 trees and palms. Alternative percentages and species combinations remain possible and should be examined in future parametric work.

All NBS coverage percentages were calculated relative to the total modeled study area of 130,457.81 m². The 5% increment was selected because it represents the remaining green coverage in the existing condition after the redevelopment-related reduction in green space, and it also provides a consistent basis for testing the additional contribution of each NBS element across the scenarios. Accordingly, 5% coverage represents approximately 6527 m² in the modeled geometry. Tree coverage refers to projected canopy area, whereas grass, green-roof, and water coverage refer to their respective horizontal surface areas. The scenarios are summarized in Table 4.

Table 4. Scenario descriptions.

Design Scenarios	Description	NBS Elements (Share %)				Purpose
		Trees Canopy Coverage (%)	Green Roof Coverage (%)	Grass Coverage (%)	Water Coverage (%)	
SC1 No NBS	No vegetation 	0%	0%	0%	0%	Reference condition without vegetation.
SC2 Existing case	Current NBS pattern on the street 	2%	0%	3%	0%	Represent the current vegetation pattern.
SC3	Adds 5% tree canopy and 5% grass 	5%	0%	5%	0%	Test additional tree shade and evapotranspiration.

SC4	Includes 5% tree canopy and 5% grass and introduces a 5% green roof 	5%	5%	5%	0%	Test whether roof greening adds pedestrian-level benefits.
SC5	Increases tree canopy to 10% with 5% grass 	10%	0%	5%	0%	Test higher tree-canopy coverage.
SC6	Retains 5% trees and 5% grass and adds 5% water surface 	5%	0%	5%	5%	Test the evaporative contribution of a water surface.
SC7	Combines all elements: 10% trees, 5% green roof, 5% grass, and 5% water 	10%	5%	5%	5%	Test the combined maximum NBS configuration.

2.9. Receptor Selection

Three receptors were placed at 1.5 m above ground to approximate the breathing and head height of standing pedestrians. Receptor 1 represents the roundabout, where the scenarios directly modify the balance of vegetation, water, and hard surfaces. Receptor 2 represents the park area, where existing greenery and open-space exposure influence the response. Receptor 3 represents the central island beside the building edge, where street-canyon geometry and sheltering can modify shade and airflow. The three locations therefore represent distinct planning conditions rather than randomly sampled points. Values were extracted at 12:00, 16:00, and 20:00 to compare midday, late-afternoon peak heat, and evening conditions (see Figure 7).

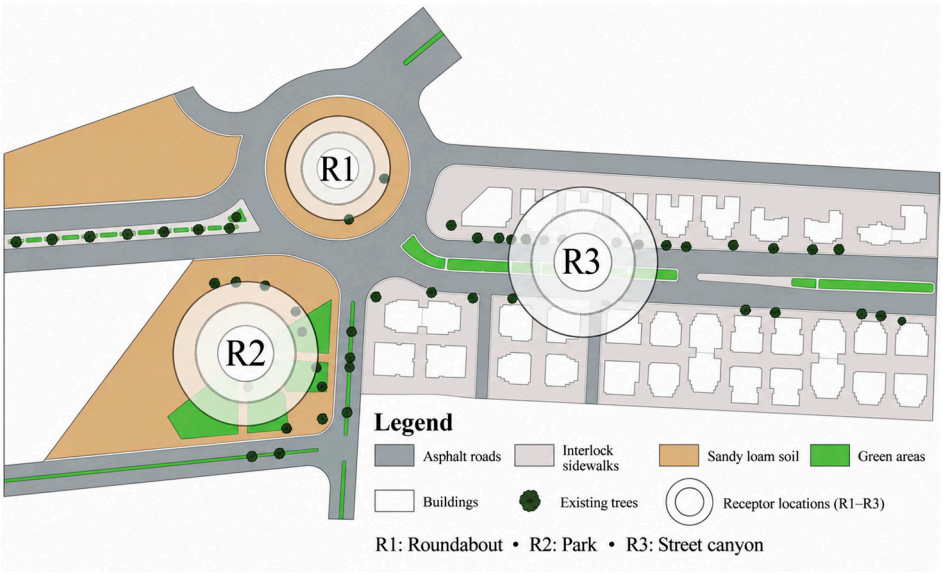


Figure 7. Placement of the three pedestrian-level receptors.

2.10. Complementary i-Tree Ecosystem-Service Assessment

The complementary ecosystem-service assessment was conducted using i-Tree MyTree version 2.30.2, powered by i-Tree Eco Engine 0.22.1 and Location Species Database 13.1.10. A representative *Ficus microcarpa* tree was modeled with a diameter at breast height (DBH) of 14.00 in (approximately 35.6 cm) and a condition classified as "Good." *Ficus microcarpa* was selected because it is commonly used in Cairo streetscapes and is adapted to harsh urban climatic conditions [34], making it a realistic candidate for shade-oriented planting and evapotranspirative cooling in the case-study context. The location setting used in MyTree was Maadi As Sarayat Al Gharbeyah, Cairo Governorate, Egypt. These inputs were used to generate the reported 20-year estimates of carbon, stormwater, and air-pollution-removal benefits (Table 5).

Table 5. Input parameters used in the i-Tree MyTree assessment.

MyTree Input	Value(s) Used
Tool	i-Tree MyTree
Version	2.30.2
Engine	i-Tree Eco Engine 0.22.1
Location Species Database	13.1.10
Species	*Ficus microcarpa*
Diameter at breast height (DBH)	14.00 in (35.6 cm)
Tree condition	Good
Location entered	Maadi As Sarayat Al Gharbeyah, Cairo Governorate, Egypt
Projection period	20 years
Estimation basis	U.S. national averages

The MyTree report indicates that the selected Egyptian location is not currently supported by the i-Tree location database; therefore, the tool used U.S. national averages to estimate the tree benefits. Consequently, the reported carbon, stormwater, air-pollution-removal, and monetary values should be interpreted as indicative estimates for the specified representative tree rather than as locally calibrated values for Cairo.

The assessment was used as a complementary planning tool rather than as a validation of ENVI-met. ENVI-met evaluates short-term pedestrian-level microclimatic effects, whereas MyTree provides longer-term estimates of tree-related ecosystem services [30]. Because the projected benefits depend on the initial tree size, condition, species, and location assumptions, the 20-year estimates are specific to the modeled input conditions and should not be generalized to all *Ficus microcarpa* trees or other street-tree conditions in Cairo.

2.11. Decision-Matrix Calculation and Normalization

The assessment followed a sequential calculation process linking NBS configuration, water demand, microclimatic performance, and ecosystem services. First, the quantities of trees, grass, green roofs, and water features were defined for each scenario. Annual irrigation demand was then estimated using the adopted requirements for trees, grass, and green roofs, while household greywater availability was calculated from the number of residential units, occupancy, an assumed greywater recovery rate of 140 L/capita/day, and 365 days per year [35]. Water-feature demand was estimated from open-water evaporation. A mean open-water evaporation rate of 2.8 mm/day for Cairo and its surroundings [36], equivalent to 1.022 m/year, resulted in an annual evaporation replacement demand of approximately 6.671 ML/year for the 6527 m^2 water surface. Total NBS water demand was compared with available greywater to determine the percentage utilized and the remaining surplus. Microclimatic performance was subsequently evaluated using the average PET across the three receptor locations and reporting times. To avoid using non-locally calibrated MyTree monetary values as a quantitative decision criterion, tree ecosystem-service performance was represented by a dimensionless proxy based on modeled tree quantity. With the same representative crown size assumed across scenarios, 70 trees corresponded to 50% of the maximum tree ecosystem-service potential and 140 trees to 100%. Because all trees were represented using the same species, size, and condition, the MyTree physical ecosystem-service estimates scale linearly with the number of trees in each scenario. Accordingly, tree number was used as a proxy for relative tree ecosystem-service potential in the decision matrix. Under the applied normalization procedure, this produces the same relative scenario scores as normalizing the corresponding non-monetary MyTree physical outputs, while avoiding reliance on U.S.-based monetary valuations that are not calibrated for Cairo. This proxy represents tree-related ecosystem services only; potential services provided by grass, green roofs, and water features were not included.

MyTree monetary outputs were retained only as illustrative co-benefit estimates and were excluded from the quantitative decision-matrix calculation. The underlying calculations used in the decision matrix are provided in Supplementary File S1.

The three components were linked through the same scenarios. ENVI-met provided thermal-comfort results, MyTree provided tree ecosystem-service estimates, and the water-balance analysis provided NBS water demand and greywater availability. Irrigation volume was not dynamically coupled with ENVI-met. Therefore, the matrix is a multi-criteria decision-support tool rather than a fully coupled model.

SC3–SC7 were ranked, while SC1 and SC2 were retained as reference conditions. Annual NBS water demand was calculated as the sum of tree, grass, green-roof, and water-feature requirements:

$$D_{NBS} = D_{trees} + D_{grass} + D_{roof} + D_{water}$$

Tree irrigation demand was estimated at 2200 L/tree/year (≈6 L/tree/day), corresponding to the upper end of the 1500–2200 L/tree/year range reported for *Ficus microcarpa* under drip irrigation [34]. Grass and green-roof irrigation demands were represented using planning-level assumptions of 2500 and 1500 L/m²/year, respectively, consistent with published irrigation requirements for comparable grass and green-roof systems [37,38]: Water-feature evaporation demand was calculated as:

$$D_{water} = A_{water} \times E_{annual} \times 1000$$

where A_{water} is the water-surface area (m²), E_{annual} is the annual evaporation depth (m/year), and the factor of 1000 converts cubic meters to liters. A mean evaporation rate of 2.8 mm/day for Cairo, equivalent to 1.022 m/year, was applied [36].

Using the adopted recoverable greywater rate of 140 L per capita per day, annual greywater availability was calculated as:

$$GW_{annual} = N_{occupants} \times 140 \times 365$$

and the remaining greywater surplus was calculated as

$$GW_{surplus} = GW_{annual} - D_{NBS}$$

Thermal-comfort performance was represented by mean PET across the selected receptors and reporting times. PET was used as the sole weighted thermal-comfort indicator to avoid double-counting air temperature, wind speed, and relative humidity. Tree ecosystem-service performance was represented by modeled tree quantity rather than MyTree monetary values; X_i denotes the number of modeled trees in scenario i and X_{max} the maximum modeled tree quantity among SC3–SC7.

To combine indicators with different units, annual water demand and PET were normalized using a lower-is-better min–max equation:

$$S_i = \frac{X_{max} - X_i}{X_{max} - X_{min}} \times 100$$

Tree ecosystem-service potential was normalized relative to the maximum modeled tree quantity:

$$S_{eco} = \frac{X_i}{X_{max}} \times 100$$

where X_i is the modeled tree quantity for scenario i, and X_{max} is the maximum modeled tree quantity. Ratio normalization was used for the tree ecosystem-service domain so that zero trees correspond to zero tree ecosystem-service potential and scenarios with 70 trees retain 50% of the potential assigned to scenarios with 140 trees.

The final composite score was calculated as:

$$C_i = (S_{Water,i} \times W_{Water}) + (S_{Microclimate,i} \times W_{Microclimate}) + (S_{Ecosystem,i} \times W_{Ecosystem})$$

where W_{Water}, $W_{Microclimate}$, and $W_{Ecosystem}$ are the weights assigned to water balance, PET, and tree ecosystem services, respectively. Four weighting profiles were tested: Equal Weighting (33.3%/33.3%/33.3%), Water Balance Priority (60%/20%/20%), Microclimate and Comfort Priority (20%/60%/20%), and Tree Ecosystem Services Priority (20%/20%/60%). Scenarios were ranked from highest to lowest composite score. The overall structure of the decision matrix is shown in Figure 8.

https://doi.org/10.3390/architecture6040201

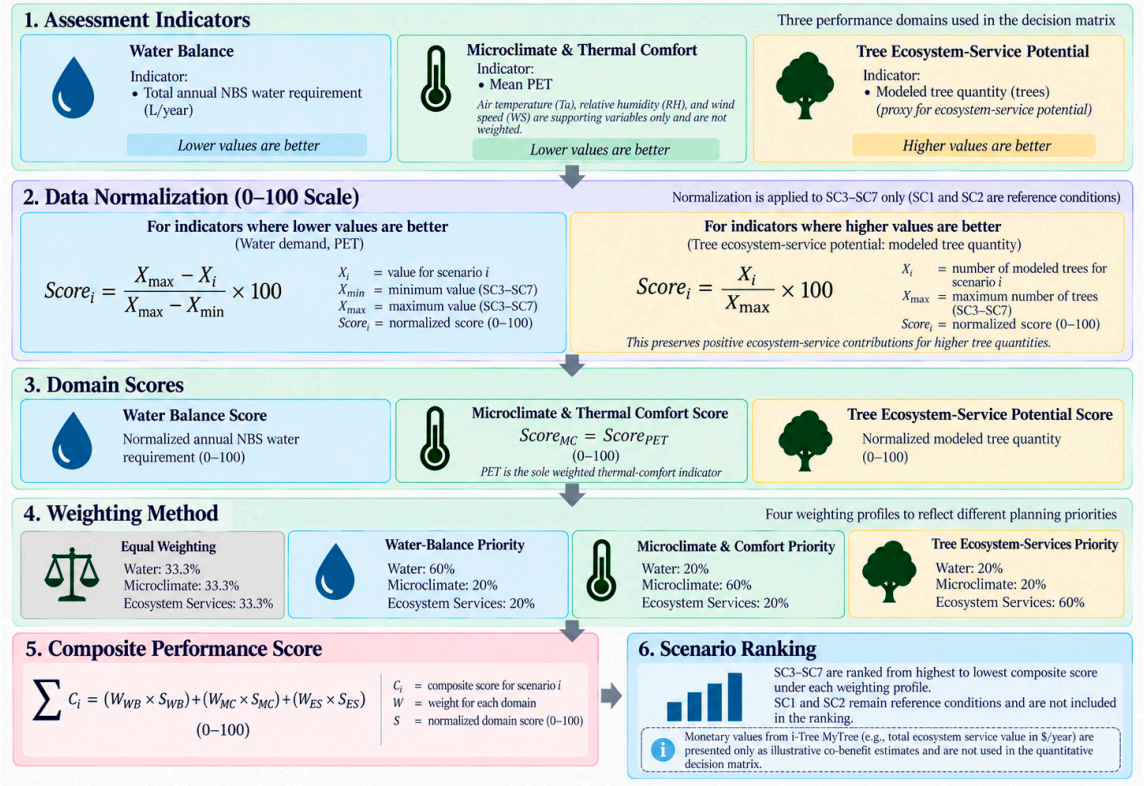


Figure 8. Integrative NBS decision matrix.

The greywater and irrigation calculations are planning-level estimates based on the adopted assumptions and were not derived from site-specific greywater measurements or a detailed treatment-system design.

3. Results

This section begins with a detailed analysis of the simulated microclimatic conditions (air temperature, wind speed, and relative humidity) across the seven NBS scenarios, including a baseline case with no vegetation, to assess and quantify the cooling and shading effects of the NBS configurations. Evaluations were conducted at 12:00, 16:00, and 20:00 at three receptor points located 1.5 m above ground to quantify the direct impact of the proposed scenarios. A comparative analysis was then performed across the different NBS scenarios to identify performance patterns at each receptor. Overall, scenarios with greater vegetation coverage generally showed lower air temperature, whereas PET differences were smaller and less consistent, with SC7 generally showing comparatively lower PET during the afternoon and evening. Scenarios with more water and vegetation tended to increase average relative humidity. Differences in average wind speed among scenarios were moderate. These results suggest that the overall effectiveness of NBS is determined by the combined influence of vegetation and moisture and their interaction with local urban settings (see Figure 9). The spatial distributions of Ta, WS, and RH for each scenario at the three reporting times are provided in Appendices A–G.

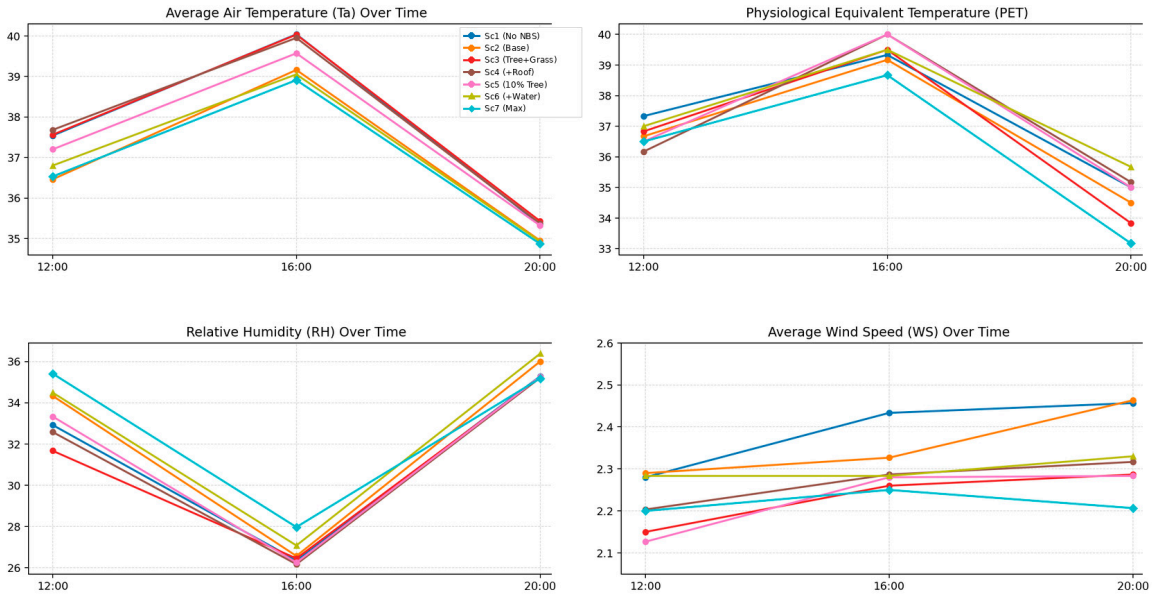


Figure 9. Thermal comfort and overall microclimatic performance across the seven NBS scenarios. Values represent means across the three pedestrian-level receptors (R1–R3) at each reporting time.

Because the 12:00 output occurs only five hours after model initialization and is therefore interpreted with greater caution (Section 2.6), the air-temperature comparison was repeated using only the 16:00 and 20:00 outputs at the three receptors (six receptor–time points per scenario). Relative to SC1, SC2 remained cooler on average (mean ΔTa = −0.47 °C; lower at 6 of 6 points), followed by SC7 (−0.35 °C; 4 of 6), SC6 (−0.28 °C; 4 of 6), and SC5 (−0.18 °C; 3 of 6). In contrast, SC3 (−0.02 °C; 1 of 6) and SC4 (+0.18 °C; 0 of 6) showed no consistent reduction. The largest later-time reductions were approximately 1.0 °C, occurring for SC2 at Receptor 3 at 16:00 and SC3 at Receptor 1 at 20:00. These results indicate that the broad scenario grouping was not dependent on the 12:00 output. An interactive dashboard visualization was created with the assistance of Claude Sonnet 5 (Anthropic) for exploratory presentation of the descriptive results; it is provided as Supplementary Material.

3.1. Receptor 1 (Location: Roundabout)

3.1.1. Air Temperature

At Receptor 1, the baseline scenario (SC1) recorded the highest midday temperature, approximately 37.6 °C at 12:00. The introduction of vegetation (SC2–SC7) reduced these peak temperatures; for example, SC5 (10% tree canopy) reached only 36.0 °C at noon, approximately 1.6 °C cooler than SC1. Afternoon (16:00) temperatures were similar across scenarios (~39–40 °C), but scenarios with more vegetation (SC5–SC7) tended to be slightly cooler (around 39.2–39.4 °C vs. 40.0 °C in SC1). By evening (20:00), temperatures dropped to approximately 34–35 °C; SC1 and SC4 were the warmest (~35.0 °C), whereas SC3 (34.0 °C) and SC7 (34.2 °C) were the coolest, followed by SC2 and SC6 (34.5 °C) and SC5 (34.7 °C). These patterns reflect the cooling influence of urban greenery, whereby tree-canopy shading and evapotranspiration reduce near-surface air temperature (see Figure 10).

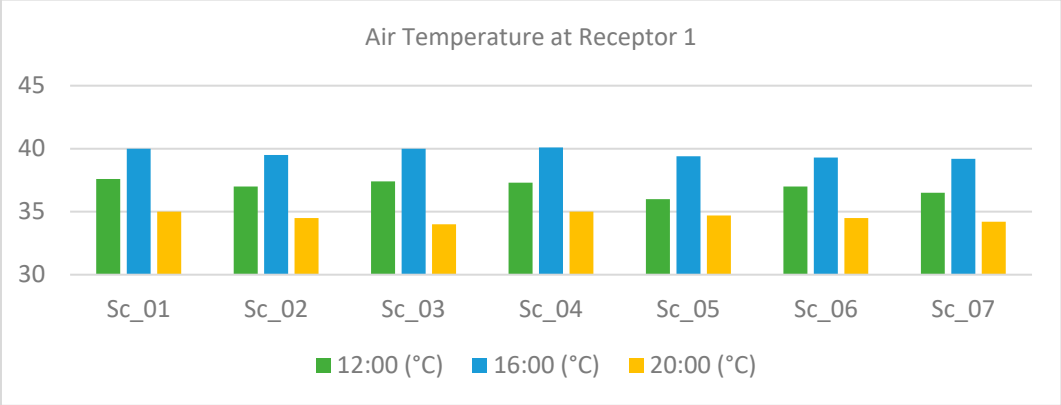


Figure 10. Air temperature at Receptor 1 across the different scenarios.

The numerical differences are modest but consistent. For example, at 12:00, the highest temperature (37.6 °C in SC1) exceeded the lowest (36.0 °C in SC5) by 1.6 °C, while afternoon differences shrank to approximately 0.9 °C across scenarios. These patterns align with the scenario descriptions: SC5 combines the highest tree cover (10%) with no green roof, so its cooling derives mainly from shade. In contrast, SC4 includes a green roof but only 5% tree cover; its higher temperatures suggest that tree canopy is the dominant cooling factor at street level, with green roofs and grass playing secondary roles. In summary, greater tree canopy lowered local air temperature, while adding water (SC6, SC7) provided additional cooling, although to a lesser extent than tree canopy.

3.1.2. Wind Speed

Wind speeds at Receptor 1 were highest at 20:00 and lowest at 12:00. At noon (12:00), wind speeds ranged from approximately 2.7 to 3.21 m/s. The highest wind speed (about 3.21 m/s) occurred in SC1 (baseline), whereas scenarios with more vegetation (SC3–SC7) were slightly lower (around 2.7–3.1 m/s). By 16:00, speeds increased to about 2.79–3.33 m/s across all scenarios; SC1 (baseline) was highest at 3.33 m/s, while SC7 was lowest at 2.79 m/s, likely because of its denser vegetation. At 20:00, wind speeds rose to 2.7–3.46 m/s, with SC6, SC1, and SC2 highest (~3.1–3.46 m/s) and SC7 lowest (~2.7 m/s). The overall differences were moderate (~0.5–0.78 m/s) and indicate a consistent pattern: scenarios with dense vegetation (trees) can slightly impede airflow, whereas more open scenarios (e.g., SC4 with a green roof but limited trees) had marginally higher wind speeds. However, all scenarios remained within a similar range (see Figure 11).

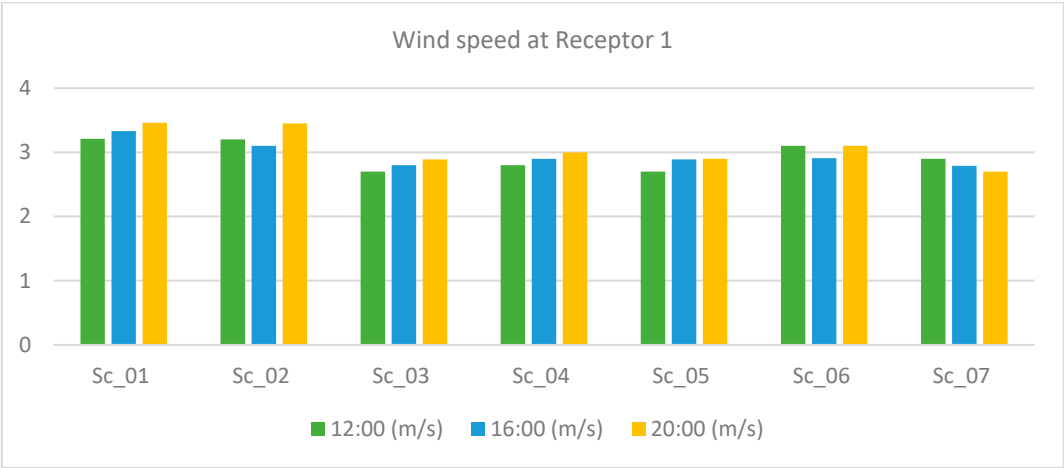


Figure 11. Wind speed at Receptor 1 across the different scenarios.

Vegetation can slightly reduce wind speed by obstructing airflow. At 12:00, SC5 (10% tree canopy) recorded 2.70 m/s, and SC7 (trees + water) recorded 2.90 m/s, both lower than scenarios with less greenery. At 20:00, SC5 remained relatively low at 2.90 m/s and SC7 at 2.70 m/s, whereas SC4, with fewer trees and a green roof, had a higher speed (3.00 m/s), indicating reduced airflow obstruction. These small changes suggest that trees increase surface roughness, which slightly slows air movement, a phenomenon frequently observed in urban green-infrastructure studies [32]. Although the wind pattern did not substantially alter the cooling effect of the scenarios, it remains a factor in outdoor thermal comfort.

3.1.3. Relative Humidity

RH at Receptor 1 followed an inverse pattern to temperature. In the mid-afternoon (16:00), RH was lowest (mid-20% range), as the hot air was drier. At 12:00, RH was in the low-30% range, and by evening (20:00), it increased to the mid-30% range. Scenarios with more moisture sources showed higher RH. For example, at 12:00, SC7 (water + trees) reached about 36% RH, versus only 30% in SC4 (trees + green roof, no water). At 16:00, SC7 reached 29%, the highest among the scenarios, while SC2 was as low as 25%. By 20:00, SC6 (with water) had the highest RH (~37%), SC7 was 36.5%, and the vegetation-poor SC2 was lowest (~34%). These differences (~3–6 percentage points) reflect evapotranspiration and evaporation: trees, grass, and especially water bodies add moisture to the air, thereby increasing humidity. The effect of water is evident, as SC6 and SC7 consistently showed higher RH (see Figure 12).

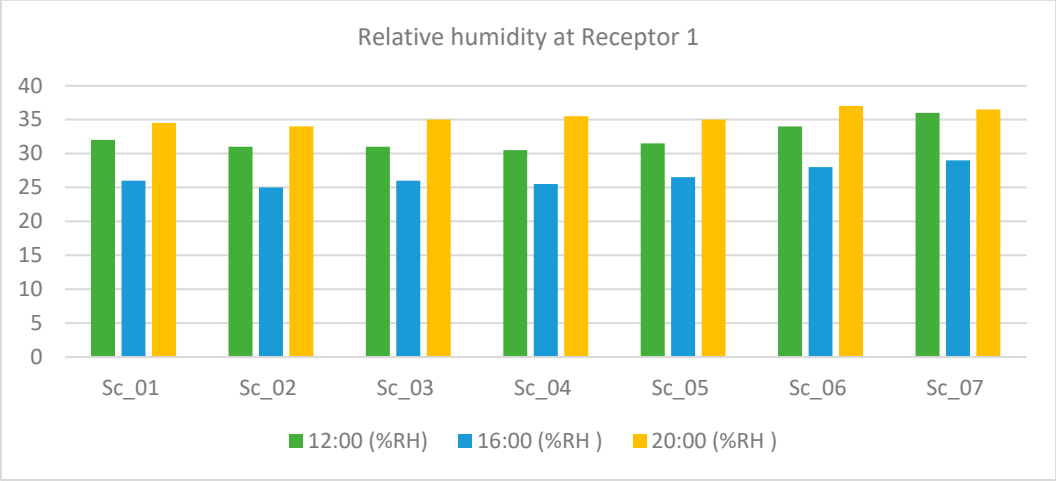


Figure 12. Relative humidity at Receptor 1 across the different scenarios.

In summary, SC6 and SC7 (with water) consistently produced higher RH, reflecting the humidifying role of water features. In contrast, SC1 and SC2, with limited vegetation and no water features, recorded the lowest RH values, indicating only modest humidity gains from existing greenery. These patterns reflect the combined effects of evapotranspiration, shading, and added moisture from trees, grass, and water. Overall, Receptor 1 experienced cooler and more humid conditions in scenarios with denser vegetation and water, which may improve thermal comfort.

3.2. Receptor 2 (Location: Park)

3.2.1. Air Temperature

At Receptor 2, temperatures were slightly higher than at Receptor 1. Midday (12:00) peaks reached 38–38.4 °C in the least-green scenario (SC1) and dropped to about 37.5–37.8 °C in SC2, SC5, SC6, and SC7, but remained at 38.0–38.2 °C in SC3 and SC4. Afternoon

values (16:00) all remained close to 40 °C, but again, the vegetation-rich scenarios were marginally lower: SC4 peaked at 40.1 °C, while SC5 and SC6 remained around 39.6 °C. Evening (20:00) values fell to approximately 34 °C: SC2 recorded about 33.8 °C (lowest) and SC4 about 34.2 °C (highest); most scenarios clustered at approximately 34.0 °C. These differences (about 0.4–1.0 °C) underscore effects similar to those at Receptor 1: greater tree cover (SC5) and the presence of water (SC6) tended to mitigate the highest temperatures (see Figure 13).

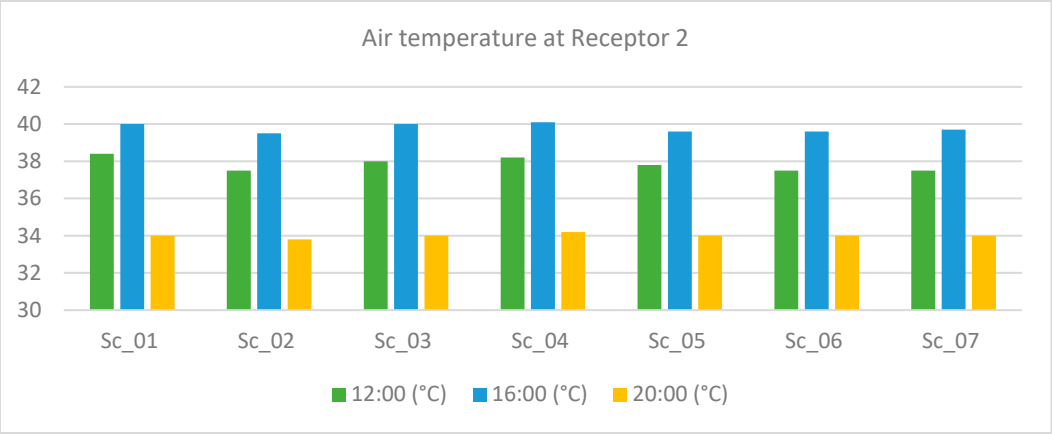


Figure 13. Air temperature at Receptor 2 across the different scenarios.

Numerically, the difference between SC1 (38.4 °C) and SC2 (37.5 °C) at noon represents a reduction of approximately 0.9 °C. At 16:00, the difference between SC4 and SC6 was only 0.5 °C. These small differences are interpreted as comparative variations within the modeled conditions rather than as distinct design effects. Nevertheless, scenarios with greater greenery, including SC5 and SC7, generally showed lower temperatures. SC5 (10% trees) was slightly cooler than SC4, while SC6 and SC7 showed similar cooling levels.

3.2.2. Wind Speed

Wind speeds at Receptor 2 were lower than at Receptor 1. At 12:00, wind speeds ranged from about 2.65 to 2.73 m/s. The strongest winds (≈2.73 m/s) occurred in SC1 and SC4, while SC2 and SC7 were lowest (~2.65 m/s). At 16:00, speeds increased to 2.77–2.82 m/s: SC5 and SC7 were about 2.77–2.79 m/s, while SC3 and SC6 were around 2.8 m/s. By 20:00, wind speeds increased to 2.87–2.91 m/s; SC1 was highest (~2.91 m/s) and SC7 was lowest (~2.87 m/s). Overall, wind-speed differences among scenarios were small, generally around 0.04–0.08 m/s. These minor variations are therefore interpreted cautiously rather than as evidence of a distinct NBS-induced airflow effect (see Figure 14).

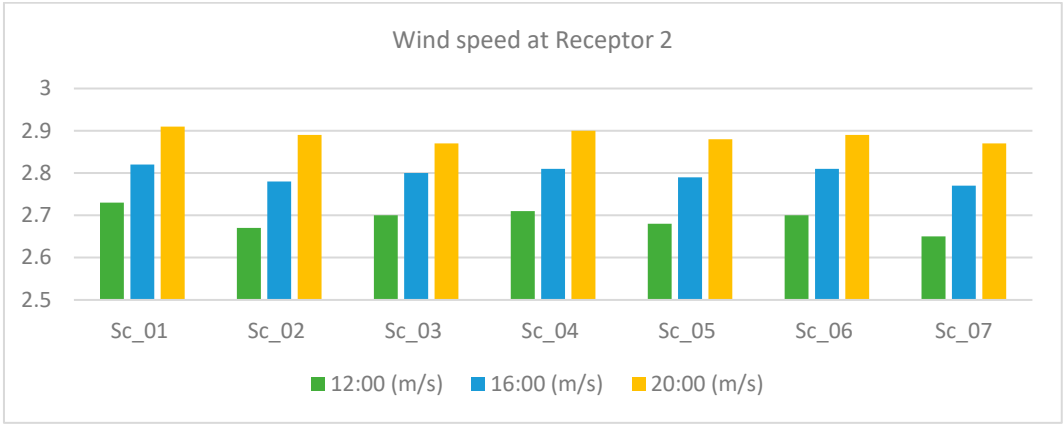


Figure 14. Wind speed at Receptor 2 across the different scenarios.

These minor wind differences indicate that airflow was broadly similar across scenarios. Trees and grass in SC5, SC6, and SC7 slightly reduced wind speed at midday and in the evening. SC4, which has fewer trees and a green roof, allowed slightly higher wind speeds. The influence of wind on temperature and humidity at this location was secondary; microclimate differences were dominated by vegetation effects rather than by ventilation changes.

3.2.3. Relative Humidity

RH at Receptor 2 showed the least variation among the receptors. At 12:00, SC2 reached the highest RH (33%) and SC3 the lowest (30%), while the others were approximately 31–32%. At 16:00, values ranged from 26% to 27%, with SC3 and SC7 highest (~27%) and SC2 and SC6 lowest (~26%). By 20:00, all scenarios converged at approximately 35% RH, reflecting cooler evening conditions. Daytime RH differences across scenarios were minimal (1–2 percentage points); the presence of a water feature (SC6, SC7) or more trees increased RH by only 1–2 percentage points. These minor changes align with the lower absolute humidity at this receptor point. Nevertheless, scenarios with vegetation maintained humidity levels slightly above baseline, which can be attributed to transpiration and surface moisture (see Figure 15).

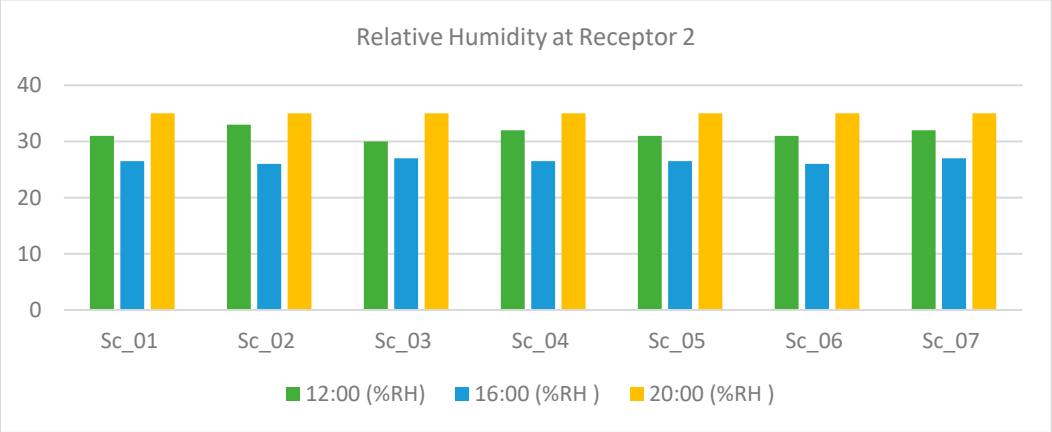


Figure 15. Relative humidity at Receptor 2 across the different scenarios.

At Receptor 2, the existing low humidity meant that additional greening had only a slight humidifying effect. The scenario with the highest tree canopy (SC5) and the water scenarios (SC6, SC7) showed higher RH at midday, reflecting modest evapotranspiration. However, after sunset, all scenarios converged, indicating that the major RH differences occurred only under strong solar radiation. The thermal-comfort implications of these small RH differences should be considered together with concurrent changes in air temperature, wind speed, and PET.

3.3. Receptor 3 (Location: Central Island)

3.3.1. Air Temperature

Receptor 3 generally experienced slightly lower daytime air temperatures than the other locations. At 12:00, SC5 recorded the lowest air temperature (~35.4 °C), closely followed by SC2 (existing case, ~35.5 °C), while SC1 recorded the highest (~36.5 °C), followed by SC7 (all NBS, ~36.2 °C) and SC4 (~36.0 °C). At 16:00, temperatures ranged from about 38.3 °C in SC2 to 39.7 °C in SC3, while by 20:00, all scenarios ranged between approximately 34.9 and 35.5 °C. These results indicate that R3 responded more to local spatial conditions than to total NBS coverage. R3 was located along the central island beside the building edge, within a deeper and more sheltered street-canyon section (Section 4.5),

where building shade lowered daytime air temperature, whereas its 20:00 values were slightly higher than those at R1 and R2 (approximately 34–35 °C), consistent with heat retention and reduced airflow in the canyon. This local setting helps explain why the scenario with the greatest overall NBS coverage did not produce the lowest temperature at this receptor and highlights the importance of canopy placement, local shading, and street-canyon geometry. Nonetheless, SC5 recorded the lowest value at 12:00, and SC5 and SC6 remained within about 0.1 °C of the lowest value at 20:00, indicating that higher tree coverage and associated NBS effects remained beneficial at certain times of day (see Figure 16).

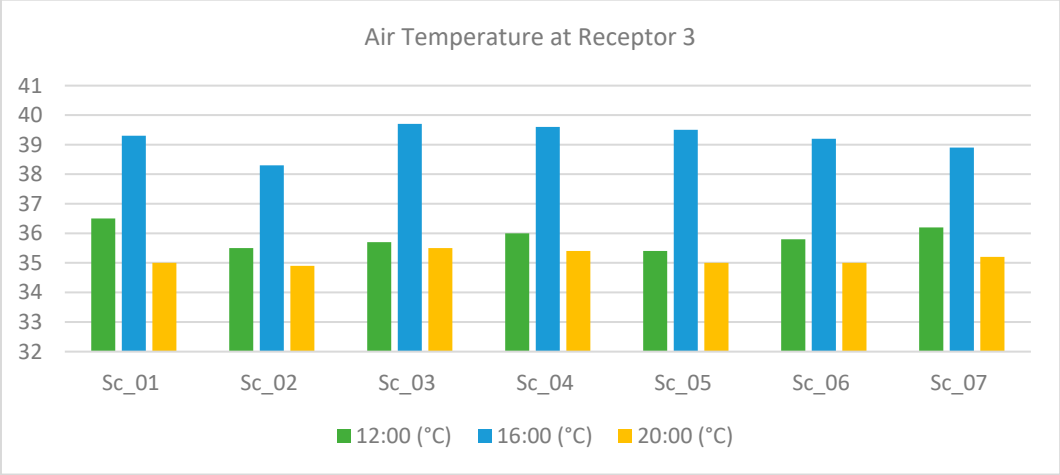


Figure 16. Air temperature at Receptor 3 across the different scenarios.

At 16:00, SC2 was approximately 1.4 °C cooler than SC3 despite SC3 having greater nominal vegetation coverage. SC5 (with 10% trees) and SC6 (which includes water) were 1.2 °C and 0.9 °C warmer than SC2, respectively, but 0.1–0.5 °C cooler than SC3 and SC4. SC1 and SC3 tended to be the hottest. This further suggests that the local microclimatic response at R3 was influenced by NBS placement, shading, and surrounding urban geometry rather than by vegetation percentage alone.

3.3.2. Wind Speed

Receptor 3 had the lowest wind speeds of the three receptor points, likely because of its more sheltered location. At 12:00, wind speeds at Receptor 3 ranged from 0.9 to 1.1 m/s; SC1 was the lowest (0.9 m/s) and SC4 the highest (1.1 m/s), reflecting the influence of the urban canyon. At 16:00, speeds increased to about 1.1–1.2 m/s, with SC7 the highest (~1.19 m/s) and SC2 the lowest (~1.10 m/s). By 20:00, wind speeds fell back to 1.0–1.1 m/s, with SC3 and SC7 at around 1.1 m/s and SC1 and SC6 at 1.0 m/s. Overall, wind speeds were nearly uniform across scenarios, with minor fluctuations. Vegetation had only subtle effects: SC7 recorded the highest afternoon wind speed at R3 (~1.19 m/s), although differences among scenarios remained small (see Figure 17).

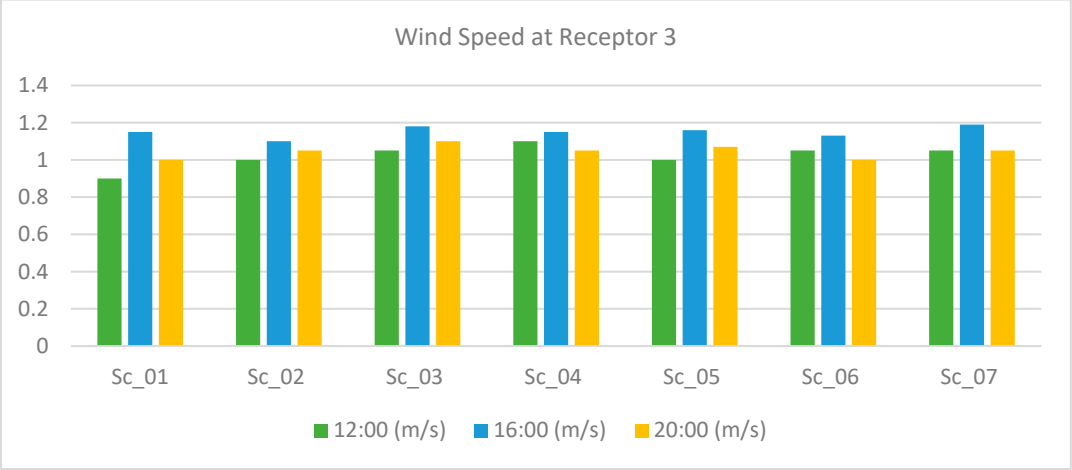


Figure 17. Wind speed at Receptor 3 across the different scenarios.

The presence of taller trees or a green roof did not substantially alter the light breezes at R3. All scenarios experienced calm conditions, so wind played little role in comfort; the observed microclimate differences were therefore associated mainly with shading and humidity rather than with ventilation.

3.3.3. Relative Humidity

At Receptor 3, RH rose sharply by evening. At 12:00, SC2 and SC7 showed the highest RH (~37%), whereas SC1 and SC3 were lowest (~34%). Afternoon values (16:00) were in the mid-20% range: SC7 was highest at 28% and SC6 lowest at 26%, a difference of two percentage points. The spatial RH map (Appendix F) indicates that the humidifying effect in SC6 was not uniformly distributed and did not extend strongly to R3, showing that the local RH response depended on receptor position relative to the water feature, vegetation, and surrounding airflow. By 20:00, RH was in the mid-30% range for all scenarios: SC2 rose to 36.5% (highest), and SC1 and SC6 remained around 34.5% (lowest). Scenarios with water or more vegetation showed the largest midday RH gain; for instance, at 12:00, RH in SC7 was 37% vs. 34% in SC1, a 3-percentage-point increase (see Figure 18).

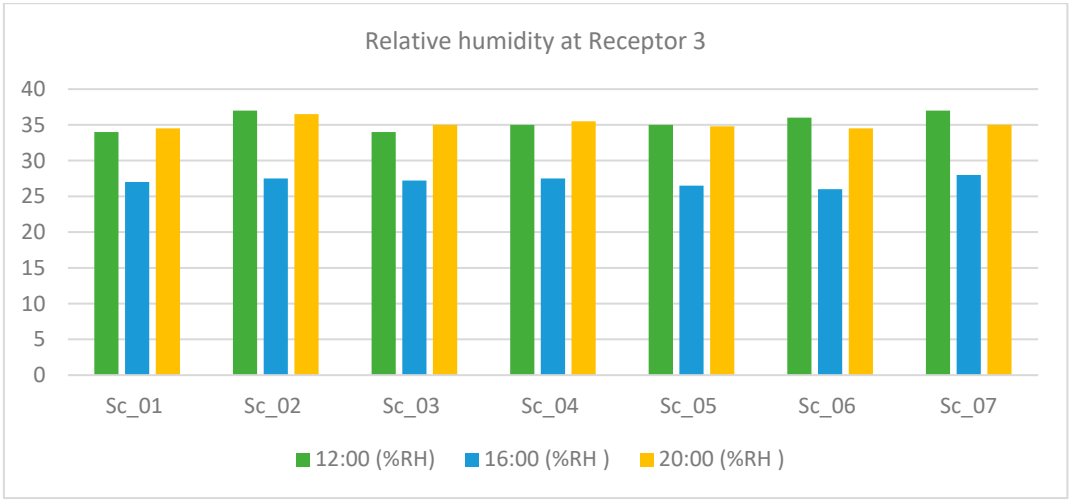


Figure 18. Relative humidity at Receptor 3 across the different scenarios.

In summary, SC2 and SC7 showed the highest RH at Receptor 3 at noon, reaching approximately 37%, compared with 34% in SC1. However, the response was not consistent across all water-containing scenarios, as SC6 recorded the lowest RH at 16:00. By

evening, humidity differences between scenarios became smaller. Overall, the results indicate that vegetation and water can increase RH, but the humidifying effect is spatially and temporally variable and depends on receptor location and local airflow.

3.4. Physiological Equivalent Temperature

The PET index was evaluated separately from air temperature and relative humidity to assess the combined thermal-comfort response of the tested scenarios. PET differences among scenarios were small, and the response was mixed: SC7 and SC3 produced the lowest mean PET, whereas SC4–SC6 did not consistently improve on the no-vegetation baseline, particularly at 16:00 (Figure 19). Averaged across the three receptors and reporting times, mean PET was 37.2 °C in SC1, compared with 36.1 °C in SC7, 36.7 °C in SC3, 36.8 °C in SC2, and 37.1–37.4 °C in SC4–SC6. At 12:00 and 16:00, PET remained within the warm-to-hot (moderate-to-strong heat-stress) ranges in most scenarios. Some evening values shifted toward the warm or slightly warm categories, particularly at Receptor 3. Even in SC5 and SC7, evening PET remained in the warm or slightly warm category. Overall, the NBS scenarios reduced PET only modestly and not uniformly relative to the baseline, and heat stress remained present during the modeled summer period (see Figure 19).

A Summary comparison of baseline-relative changes in Ta, PET, RH, and WS for all scenarios and receptors, together with summary graphs, is provided in Supplementary File S2.

3.5. Sensitivity Analysis Results

The targeted one-at-a-time (OAT) sensitivity analysis showed that the relative response of SC5 and SC1 varied with meteorological forcing, receptor location, and time of day. Across the four perturbed conditions, comprising 36 receptor–time–condition comparisons (Table 6), SC5 produced lower air temperature (Ta) than SC1 in 21 cases (58.3%), with an overall mean ΔTa of approximately −0.01 °C. This near-zero overall mean reflects offsetting responses among the individual forcing conditions. Under low-temperature forcing, SC5 was cooler in 7 of 9 comparisons (mean ΔTa = −0.23 °C). Under high-temperature forcing, the response reversed, with SC5 warmer than SC1 in all 9 comparisons (mean ΔTa = +1.03 °C). Under low-wind and high-wind forcing, SC5 was cooler in 6 of 9 and 8 of 9 comparisons, with mean ΔTa values of −0.72 °C and −0.11 °C, respectively.

PET also showed a forcing-dependent response. Across all 36 comparisons, SC5 had lower PET than SC1 in 20 cases (55.6%), with an overall mean ΔPET of −0.81 °C. Mean ΔPET values were −1.30 °C under low-temperature forcing, +0.59 °C under high-temperature forcing, −1.27 °C under low-wind forcing, and −1.25 °C under high-wind forcing. The corresponding numbers of comparisons in which SC5 had lower PET were 5 of 9, 3 of 9, 7 of 9, and 5 of 9, respectively. Thus, the high-temperature perturbation differed from the other three conditions by producing, on average, both higher Ta and higher PET in SC5 relative to SC1.

Relative humidity (RH) and local wind speed (WS) also varied between SC5 and SC1. Mean ΔRH was +1.24 percentage points (pp) under low-temperature forcing, −2.11 pp under high-temperature forcing, +3.26 pp under low-wind forcing, and +0.60 pp under high-wind forcing; the overall mean across the four conditions was +0.75 pp. Mean ΔWS was −0.05, −0.13, −0.04, and −0.07 m/s under the same four conditions, respectively, with an overall mean of −0.07 m/s. Overall, the sensitivity analysis does not indicate a uniform thermal advantage for SC5 under every boundary condition. Instead, the magnitude and, in some cases, the direction of the SC5–SC1 response depended on meteorological forcing, receptor location, and time of day. Detailed receptor-level values and calculations are provided in Supplementary File S5.

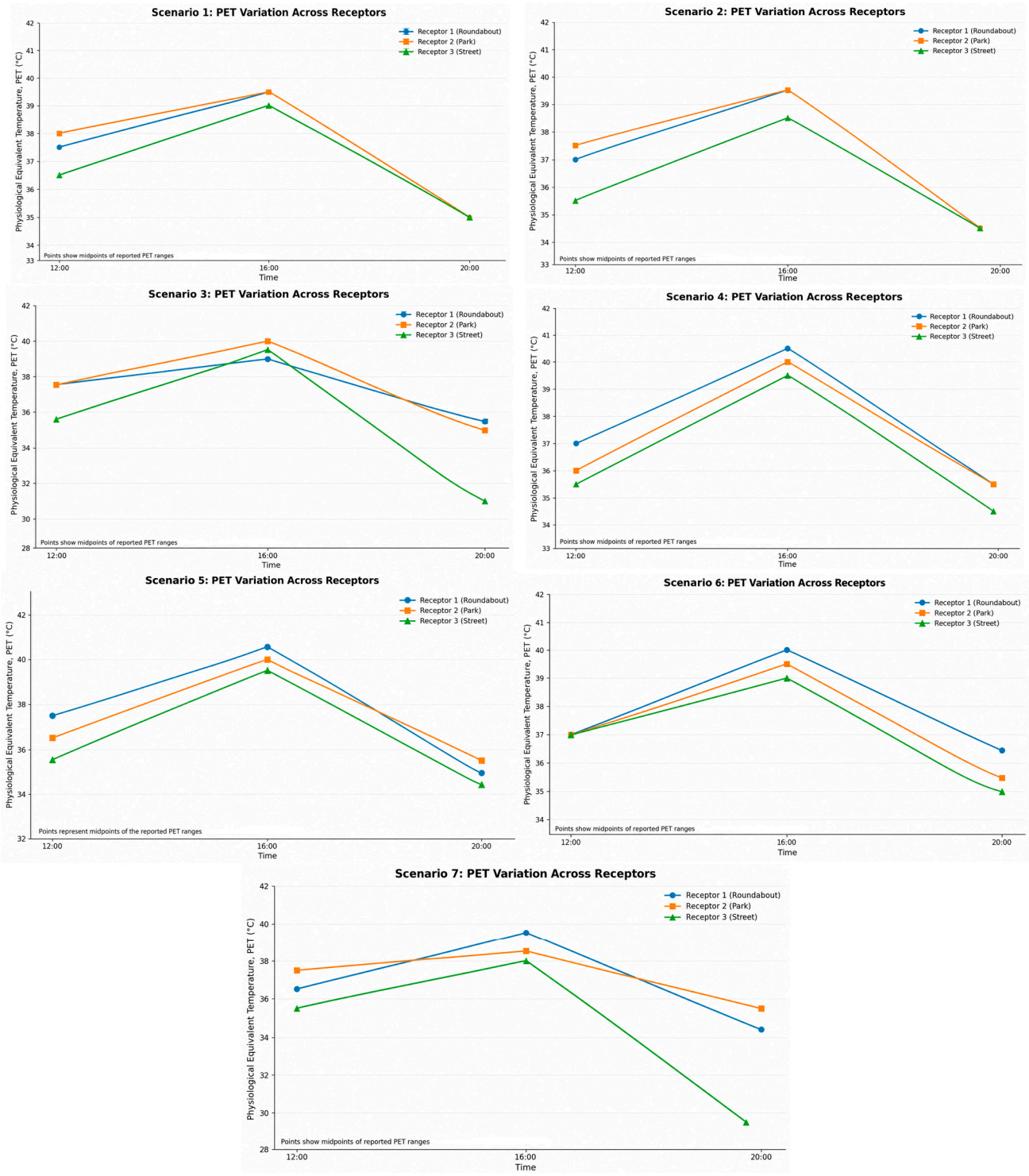


Figure 19. PET results across the seven scenarios.

Table 6. Summary of the OAT sensitivity analysis for SC5 relative to SC1 (SC5 − SC1).

Condition	Mean ΔTa (°C)	SC5 Lower Ta	Mean ΔRH (pp)	Mean ΔWS (m/s)	Mean ΔPET (°C)	SC5 Lower PET
Low temperature	−0.23	7/9 (77.8%)	+1.24	−0.05	−1.30	5/9 (55.6%)
High temperature	+1.03	0/9 (0.0%)	−2.11	−0.13	+0.59	3/9 (33.3%)
Low wind	−0.72	6/9 (66.7%)	+3.26	−0.04	−1.27	7/9 (77.8%)
High wind	−0.11	8/9 (88.9%)	+0.60	−0.07	−1.25	5/9 (55.6%)
Overall	−0.01	21/36 (58.3%)	+0.75	−0.07	−0.81	20/36 (55.6%)

Note: Δ = SC5 − SC1. Negative ΔTa and ΔPET indicate lower Ta and PET in SC5, respectively. Positive ΔRH indicates higher RH in SC5 and is reported in percentage points (pp). Negative ΔWS indicates lower local wind speed in SC5. The overall row represents 36 receptor–time–condition comparisons.

3.6. Decision-Matrix Results and Weighting Analysis

The decision matrix compares SC3–SC7 across three domains: annual NBS water demand, pedestrian thermal comfort represented by mean PET, and tree ecosystem-service potential represented by modeled tree quantity. SC1 and SC2 were retained as reference conditions and were not included in the scenario ranking. Four weighting profiles were applied to examine how changes in planning priorities affect scenario performance. The resulting composite scores and ranks are summarized in Table 7, and detailed calculations are provided in Supplementary File S1.

Under Equal Weighting, SC5 achieved the highest composite score (72.19), followed by SC3 (67.49), SC7 (66.67), SC4 (37.58), and SC6 (36.62). Under Water Balance Priority, SC5 remained the highest-ranked scenario (82.94), followed by SC3 (80.50), SC6 (45.91), SC7 (40.00), and SC4 (38.98). When Microclimate and Comfort was prioritized, SC7 ranked first (80.00), followed by SC3 (61.49), SC5 (50.31), SC4 (31.22), and SC6 (21.97). Under Tree Ecosystem Services Priority, SC5 ranked first (83.31), followed by SC7 (80.00), SC3 (60.50), SC4 (42.55), and SC6 (41.97). The weighting analysis demonstrates that no single scenario performs best under every planning objective. SC5 performs most strongly when water efficiency, balanced performance, or tree ecosystem services are given greater weight, whereas SC7 becomes the highest-ranked option when pedestrian thermal comfort is prioritized. The results therefore indicate that scenario preference depends on the relative importance assigned to water demand, thermal comfort, and tree ecosystem-service benefits.

For example, under Equal Weighting, SC5 received normalized scores of 99.07 for water balance, 17.49 for PET, and 100 for tree ecosystem services. With equal weights assigned to the three domains, the composite score was calculated as (99.07 + 17.49 + 100)/3 = 72.19.

Table 7. Decision-matrix composite scores and ranks for SC3–SC7 under the four weighting profiles.

Scenario	Equal Weighting	Water Balance Priority	Microclimate and Comfort Priority	Tree Ecosystem Services Priority
SC3	67.49 (2)	80.50 (2)	61.49 (2)	60.50 (3)
SC4	37.58 (4)	38.98 (5)	31.22 (4)	42.55 (4)
SC5	72.19 (1)	82.94 (1)	50.31 (3)	83.31 (1)
SC6	36.62 (5)	45.91 (3)	21.97 (5)	41.97 (5)
SC7	66.67 (3)	40.00 (4)	80.00 (1)	80.00 (2)

Values in parentheses indicate rank within SC3–SC7. SC1 and SC2 are reference conditions and are not ranked. Higher normalized and composite scores indicate stronger performance under the specified decision criteria and weighting profile.

4. Discussion

4.1. Performance of Tree-Based Scenarios

The ENVI-met simulation results indicate that NBS can play an important role in improving the outdoor microclimate in hot-arid cities such as Cairo. Analysis of the seven scenarios indicates that increased vegetation cover, particularly tree canopy, contributes to measurable reductions in air temperature and to modest, location-dependent changes

in outdoor thermal comfort [39,40]. These findings are consistent with previous studies highlighting the cooling potential of urban vegetation in mitigating the UHI effect [41,42].

At midday (12:00), scenarios with greater vegetation, especially SC5 with 10% tree cover, generally showed lower air temperatures than scenarios with less vegetation, such as SC1 and SC2; averaged across the three receptors, SC5 recorded the lowest midday value (36.4 °C, compared with 37.5 °C in SC1 and 36.7 °C in SC2). At 16:00 and 20:00, however, SC2 remained cooler on average than SC5 (Section 3). At Receptor 1, the midday difference between the baseline scenario without vegetation (SC1) and the higher-tree-cover scenario (SC5) was about 1.6 °C. This finding indicates that tree shading and evapotranspiration play an important role in cooling the urban microclimate. This agrees with earlier studies showing that tree canopies enhance evaporative cooling processes and reduce pedestrian exposure to solar radiation [43].

The findings also indicate that grass surfaces and green roofs provide additional cooling benefits; however, their effects appear smaller than those of tree-canopy cover. Green roofs can help reduce heat storage at the building and surface levels; however, their cooling effect is concentrated primarily at the roof level. Grass can enhance surface permeability and evapotranspiration but provides little direct shade, so both interventions generally have a more limited and less immediate influence on pedestrian-level thermal conditions [44].

Overall, the results indicate that within the modeled scenarios, greater tree canopy generally lowered pedestrian-level air temperature, most clearly at midday, while additional elements such as green roofs and grass contributed supplementary benefits [45].

4.2. Contextual Comparison with Selected ENVI-Met/NBS Studies

The results of the present study are generally consistent with prior ENVI-met and NBS studies, and they also highlight the importance of local urban context. In a case study of El-Nozha, Cairo, Elbardisy et al. [14] found that optimized urban tree placement can reduce air temperature and PET, particularly when solar radiation exposure is reduced. Similarly, Gomaa et al. [32] investigated enhanced tree coverage combined with grass in a low-density hot-arid residential area and reported reductions in air temperature of roughly 0.2–0.92 °C. These values are within the range of the lower and intermediate cooling effects obtained in the present study. Kaçmaz Akkurt and Şemsiyeci [8] examined trees and other NBS scenarios in the Mediterranean climate of İzmir and reported temperature decreases of about 0.08–1.90 °C, depending on the scenario and receptor placement. The broad range identified in their study emphasizes that the effectiveness of NBS is strongly spatially dependent and influenced by the surrounding urban configuration. The NBS configurations (trees, grass, green roofs, and water) modeled for the road-widened Zahraa El Maadi Street in this study resulted in reductions in air temperature of roughly 0.4–1.6 °C, depending on receptor location and time of day (up to about 1.0 °C when only the 16:00 and 20:00 outputs, which lie beyond the initialization period, are considered). This range is therefore consistent with the magnitude of cooling reported in comparable simulation studies. However, the key contribution of the current research is not only to show the possible cooling effects but also to assess NBSs as a design response to green-space loss associated with road widening. Comparison with prior studies suggests that NBS efficacy should not be judged by a single maximum cooling value; rather, the intervention type, site, urban morphology, and receptor-specific exposure substantially influence the resulting microclimatic response.

4.3. Thermal Comfort and Planning Implications

PET is a widely used indicator of outdoor thermal comfort because it integrates multiple environmental factors, such as air temperature, wind speed, humidity, and radiation, into a single index [29].

However, within the modeled summer day, site geometry, and receptor locations, the cooling effects of the tested NBS interventions remained limited. Even in the better-performing scenarios, including SC3 and SC7, daytime PET remained within elevated heat-stress categories.

This indicates that although NBS are important mitigation measures, substantial improvement in thermal comfort may require integration with additional urban-design measures, such as shading devices, high-reflectivity materials, and improved urban ventilation. Overall, the NBS scenarios reduced thermal stress incrementally but did not eliminate heat stress during the modeled severe-summer period [39].

4.4. Integration of ENVI-Met and i-Tree

The i-Tree analysis supports the planning argument by identifying co-benefits of the tree-based intervention. For the representative *Ficus microcarpa* tree, MyTree estimated the environmental benefits provided over 20 years. The tree was estimated to provide a total monetary value of approximately USD 101.16 over this period. These benefits included carbon dioxide uptake, with the monetary value associated with carbon removal estimated at USD 80.45, corresponding to approximately 168.7 kg of carbon sequestered (equivalent to 618.4 kg of CO_2) [30].

The tree was also estimated to provide stormwater benefits valued at USD 8.62, including approximately 964.34 gallons (≈3650 L) of avoided runoff and 17,104.1 gallons (≈64,750 L) of intercepted rainfall. Because these stormwater estimates were generated using U.S. national-average conditions rather than Cairo precipitation, they should not be interpreted as expected stormwater performance for the case-study site. In addition, air-pollution-removal benefits were estimated at USD 12.09, including the removal of carbon monoxide, ozone, nitrogen dioxide, sulfur dioxide, and $PM_{2.5}$. Overall, these estimates suggest that a single established tree can provide long-term carbon, stormwater-management, and air-quality benefits in an urban environment (see Figure 20).

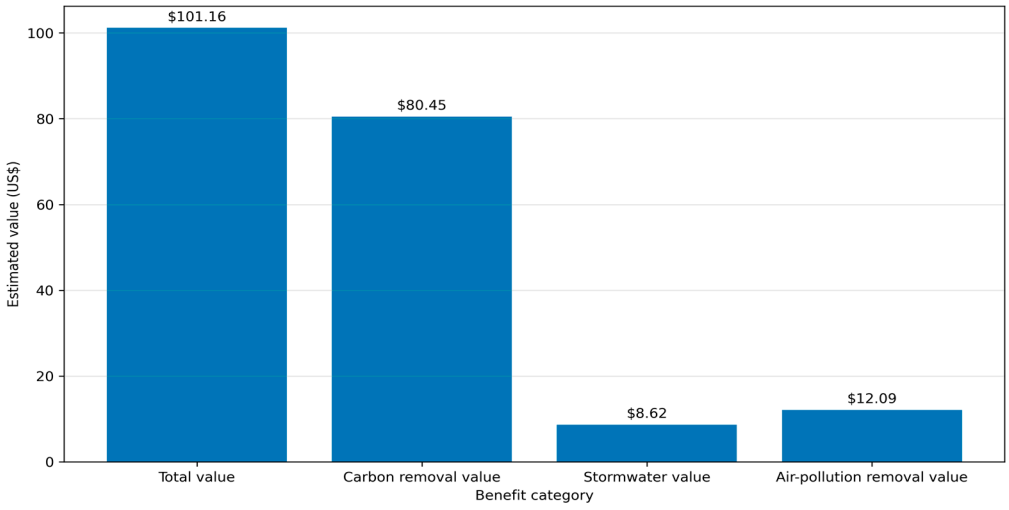


Figure 20. Illustrative 20-year MyTree ecosystem-service estimates for the modeled *Ficus microcarpa* tree, based on U.S. national averages and not locally calibrated for Cairo.

However, the MyTree estimates should be interpreted cautiously because the selected Cairo location is not currently supported by the MyTree location database, and U.S.

national averages were therefore used to estimate the benefits. Accordingly, the reported ecosystem-service and monetary values are illustrative rather than locally calibrated for Cairo and depend on the assumed tree size, condition, species, and location settings. The integration of ENVI-met and MyTree therefore provides complementary rather than directly comparable information: ENVI-met evaluates short-term effects on air temperature, wind speed, relative humidity, and PET, while MyTree provides an indication of longer-term carbon, stormwater, and air-quality co-benefits. These MyTree monetary outputs were retained only as illustrative co-benefit estimates and were excluded from the quantitative decision-matrix calculation.

Ficus microcarpa was used because it is a realistic and commonly planted streetscape species in Cairo. Nevertheless, species selection should be expanded in future research to compare canopy sizes, leaf-area density, irrigation demand, rooting space, drought tolerance, maintenance requirements, biodiversity value, and potential conflicts with urban infrastructure [34].

4.5. Wind and Humidity Trade-Offs

Vegetation can reduce beneficial airflow by increasing surface roughness, especially in areas where rows of trees are dense or not aligned with the prevailing wind direction [32]. The three receptors correspond to different microclimatic conditions affecting the wind–humidity response. Receptor 1, located in an open roundabout with no existing trees, experienced greater exposure to solar radiation and unobstructed airflow. Receptor 2, located in a park with only a few trees, showed limited vegetation-induced modification of wind conditions.

In contrast, Receptor 3 is situated within an urban fabric characterized by a higher aspect ratio and, consequently, deeper street canyons. This configuration reduces solar penetration, so R3 generally experienced slightly lower daytime air temperatures than the other receptors, while its more sheltered form also limited airflow. This suggests that urban morphology and spatial layout play a critical role in determining the effectiveness of NBS strategies, as building geometry influences shading patterns, airflow distribution, and heat storage within urban environments.

Water-based NBSs can provide evaporative cooling but simultaneously increase RH, creating a temperature–humidity trade-off [41]. In this study, the water scenarios raised RH but did not consistently produce the lowest PET, suggesting that humidity partly limited the thermal-comfort benefit. However, the humidifying effect was spatially non-uniform; at R3, SC6 recorded the lowest RH at 16:00 despite including a water feature, indicating that evaporative effects depend on receptor location and local airflow.

Overall, RH varied only slightly among the scenarios: the addition of water features increased humidity levels through evaporation and surface moisture, but these increases were small, typically 1–2 percentage points at R2 and R3 and up to ~6 percentage points at R1, reflecting the generally dry atmospheric conditions characteristic of Cairo's hot-arid climate. The thermal effect of this modest RH increase depends on concurrent changes in air temperature, radiation, and airflow; in the present study, the water scenarios did not consistently produce lower PET. Their effectiveness therefore depends on local airflow and urban morphology [21]. Accordingly, water features are better considered a supplementary, site-specific strategy rather than a primary large-scale cooling intervention.

4.6. NBS and Greywater Reuse

In major urban developments in hot-arid regions such as Egypt, planners have traditionally focused on street and mobility networks while giving limited attention to broader

environmental impacts. Given this harsh climate, it is critical to move beyond conventional functionality and integrate NBS that act as environmental remedies within residential areas.

The integration of NBS with greywater treatment provides an opportunity to address one of the main limitations of greening strategies in hot-arid cities: water scarcity. Treated household greywater can provide an alternative irrigation source for trees, grass, and green roofs, reducing dependence on potable water while supporting the evapotranspiration and shading functions required for microclimatic cooling [35]. In this way, greywater reuse can transform NBS from a water-consuming intervention into part of a more circular urban water-management system (see Figure 21). However, its application requires appropriate treatment, water-quality control, efficient irrigation, and consideration of maintenance requirements [46].

The study does not include detailed sizing or design of greywater collection, storage, treatment, pumping, or distribution infrastructure; therefore, the proposed system should be interpreted as a conceptual resource-circularity strategy.

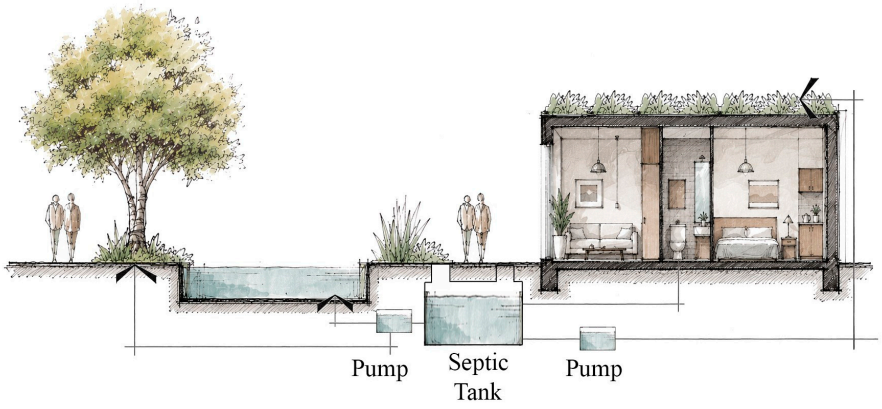


Figure 21. Conceptual cross-section showing how the proposed greywater–NBS system could be implemented.

4.7. Urban Planning and Design Implications: An Integrative NBS Framework for Hot-Arid Regions

The study area lies in a hot-arid region with specific characteristics driven by climatic variables, such as high temperatures and intense heat exposure [9]. NBSs are important elements to consider in urban design, and many studies in hot-arid regions illustrate their usefulness and importance in this context [12]. However, there are various obstacles, most notably water scarcity and excessive heat, which negatively affect the existing landscape and may entail higher maintenance costs or substantial water use, making such solutions difficult to accommodate. The proposed framework was therefore developed in two phases.

The first phase involved the use of simulation tools, which support decision-making at the initial stage and help ensure that the design performs effectively under harsh environmental conditions. In this phase, we considered urban redevelopment scenarios, such as road widening or green-space reduction, that may adversely impact land-surface temperature and pedestrian-level comfort. Based on street attributes and the surrounding landscape, we then developed a set of scenarios combining different NBS elements, including street trees, grass, green roofs, and water features. Subsequently, simulations were performed to assess the effects on thermal comfort and meteorological variables, such as air temperature, humidity, and wind. The i-Tree MyTree tool was then used to estimate the air-pollution-removal and other ecosystem-service co-benefits of the tree-

based scenarios, complementing the microclimatic assessment undertaken with ENVI-met.

The second phase addressed resource feasibility, particularly the water requirements of NBS interventions under hot-arid conditions. Water-containing scenarios provided microclimatic benefits but also required additional water to compensate for evaporation; therefore, their overall suitability depends on the planning priority and the availability of non-potable water resources. Given the water scarcity associated with these harsh climatic conditions, the framework draws on local contextual assets, making contextualization crucial. When water features are implemented in residential communities, a greywater collection system can be established using water from washbasins, sinks, showers, and other household sources.

This water can be treated using simple techniques such as constructed wetlands, which can serve as water features while simultaneously improving air quality, increasing humidity, and enhancing overall environmental quality [46]. The treated water can then be used for green-roof and tree irrigation with a drip irrigation system to minimize water use [34]. Finally, the technical and economic feasibility of such a system would require a project-specific assessment of collection, treatment, storage, pumping, distribution, operation, and maintenance requirements (see Figure 22).

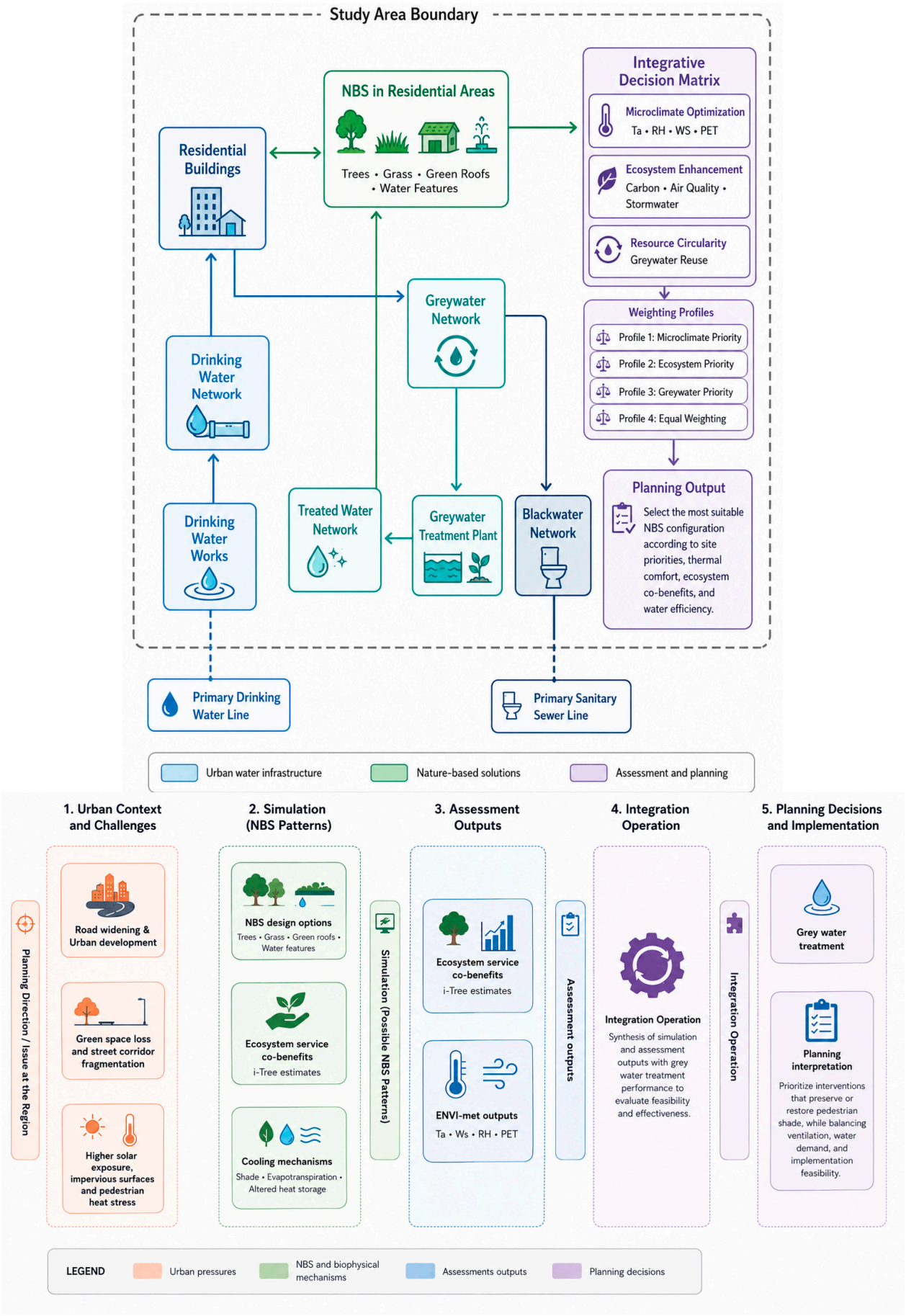
To address this challenge, an integrative decision matrix was developed to guide planners in incorporating these solutions within the urban environment. The framework includes a thematic weighting analysis that demonstrates how existing site assets can be used to enhance overall living conditions. Specifically, a decision-support toolkit was formulated, structured around three core thematic dimensions:

- Microclimate and Comfort Performance: Enhancing outdoor microclimates and human thermal comfort in pedestrian spaces.
- Ecosystem Enhancement: Improving the urban ecosystem by reducing air pollution, sequestering carbon, and optimizing stormwater management and runoff control.
- Resource Circularity: Capturing excess household greywater for reuse in urban irrigation systems—a vital strategy for water-scarce, hot-arid regions such as Egypt.

To operationalize this framework for different planning priorities, the model is structured into four distinct thematic weighting profiles:

1. Microclimate and Comfort Priority: Emphasizes enhancing the outdoor microclimate and human thermal comfort as the primary objective, with the other two factors weighted equally.
2. Tree Ecosystem Services Priority: Assigns the largest weight to urban ecosystem enhancement, with the other two factors weighted equally.
3. Water Balance Priority: Prioritizes lower annual NBS water demand and reduced use of the available greywater supply as the core objective, with equal weight given to the other two factors.
4. Equal Weighting: Applies a balanced approach, assigning equal weight to all three core dimensions.

The weighting analysis indicates that scenario preference changes according to the selected planning priority. SC5 ranked first under Equal Weighting, Water Balance Priority, and Tree Ecosystem Services Priority, whereas SC7 ranked first when Microclimate and Comfort was prioritized. Therefore, the decision matrix should be interpreted as a decision-support tool rather than as a means of identifying a universally optimal NBS configuration.



https://doi.org/10.3390/architecture6040201

Figure 22. Conceptual framework linking road-induced green-space loss, NBS mechanisms, microclimate assessment, ecosystem-service co-benefits, and planning decisions (**top**), and the study-area boundary for the greywater treatment system (**bottom**).

The decision matrix provides a structured decision-support framework for the modeled case study context; however, its applicability to other hot-arid urban environments requires further validation across different urban densities, green-infrastructure configurations, and environmental conditions. These constraints present valuable opportunities for future research, which could investigate the application of the decision matrix across diverse urban typologies and varying environmental contexts. The complete decision matrix is provided in Supplementary File S1 (see Figure 22).

4.8. Sensitivity Analysis and Robustness

The sensitivity analysis reinforces the interpretation that the microclimatic effect of additional tree canopy is conditional rather than uniform. Although SC5 generally showed favorable thermal responses under several perturbations, the direction and magnitude of the SC5–SC1 difference changed with the imposed meteorological forcing, receptor location, and time of day. This indicates that tree-canopy performance should not be interpreted as an intrinsic property of canopy percentage alone; rather, it emerges from the interaction among vegetation, local urban form, and the prevailing atmospheric conditions [45].

The contrasting responses under the temperature and wind perturbations are particularly relevant to hot-arid street design. Changes in wind forcing alter local ventilation and the interaction between vegetation and airflow [33,45], while changes in temperature forcing modify the thermal background within which shading and evapotranspirative effects operate. The reversal observed under the high-temperature perturbation therefore cautions against assuming that a configuration that performs well under one meteorological condition will necessarily retain the same advantage under more severe thermal forcing. Similarly, the different responses under low- and high-wind conditions show that preserving beneficial airflow can be as important as increasing shade [32].

The distinction between air-temperature and PET responses also has an important planning implication. A reduction in air temperature does not necessarily produce an equivalent improvement in thermal comfort because PET reflects the combined influence of air temperature, humidity, wind speed, and radiation-related thermal load. The sensitivity results therefore support the broader findings of this study that NBS performance should be evaluated using more than one microclimatic indicator and that maximum tree-canopy coverage is not, by itself, a sufficient criterion for selecting the preferred design [33,45].

These findings provide evidence of conditional robustness rather than proof that SC5 is uniformly superior. The OAT analysis strengthens the controlled comparison by showing how the relative SC1–SC5 response changes when key meteorological inputs are perturbed. From a planning perspective, the results support a context-sensitive approach in which tree placement, canopy coverage, urban geometry, ventilation pathways, and water requirements are considered together [33,45]. This interpretation is consistent with the decision-matrix results, which likewise show that the preferred NBS configuration depends on the planning objective and the assumptions applied.

5. Limitations and Future Research

The main limitation of this research is its reliance on ENVI-met simulation without site-specific field validation. This approach may not fully capture the dynamic and complex nature of real urban microclimate conditions, particularly given the use of a single

simulation day and a limited number of receptor points. In addition, the 12:00 output was obtained five hours after model initialization and is therefore interpreted with greater caution than the 16:00 and 20:00 outputs. To address uncertainty in the meteorological boundary conditions, a targeted one-at-a-time (OAT) sensitivity analysis was conducted for SC1 and SC5 by perturbing air-temperature forcing by ±2 °C and changing the baseline inflow wind speed of 4.5 m/s to 3.0 and 6.0 m/s. However, the analysis was limited to two representative scenarios and two meteorological parameters and therefore does not constitute a comprehensive uncertainty analysis of all ENVI-met inputs. Accordingly, the results should be interpreted primarily as comparative scenario-based evidence rather than as site-calibrated predictions of absolute microclimatic conditions.

Vegetation was modeled using a fixed canopy representation based mainly on *Ficus microcarpa*, without accounting for differences in tree-species characteristics. Factors such as leaf-area density, canopy structure, and evapotranspiration rates can vary considerably among species and may strongly influence cooling performance, particularly in hot-arid climates. The water-feature demand was also estimated using a published mean open-water evaporation rate for Cairo rather than site-specific evaporation measurements and should therefore be regarded as a planning-level estimate. Tree, grass, and green-roof irrigation demands were likewise represented using planning-level rates, and the Water Balance Priority ranking may be sensitive to the assumed irrigation demands. Site-specific irrigation data should therefore be used when applying the decision matrix in practice.

Future research should combine site-specific field measurements with broader multi-parameter sensitivity testing (including relative humidity, vegetation characteristics, surface properties, and model-resolution settings), continuous multi-day and multi-season simulations, and species-specific vegetation analyses to improve model reliability and evaluate performance under different wind, seasonal, and heatwave conditions. Future work should also explore dynamically coupling irrigation-dependent vegetation performance with ENVI-met simulations to better represent the interactions between water availability and microclimatic response.

Additionally, for the present MyTree assessment, Cairo was not supported by the i-Tree location database; consequently, U.S. national averages were used to estimate the ecosystem-service and monetary benefits. These outputs are therefore not locally calibrated for Egyptian conditions. The monetary outputs were retained only as illustrative co-benefit estimates and were excluded from the quantitative decision-matrix scoring. This limitation is particularly important for the stormwater estimates, which reflect U.S.-average climatic assumptions and should not be interpreted as representative of rainfall interception or runoff reduction in Cairo. Future research should recalculate these services using locally calibrated precipitation, pollution, and economic data.

Finally, ENVI-met represented a one-day microclimatic condition with fixed canopy geometry, whereas i-Tree estimated longer-term tree benefits. The two tools therefore operate at different temporal scales and were integrated only as complementary planning indicators rather than as directly equivalent measures.

6. Conclusions

This study compared seven simulated NBS configurations for a road-widened street in Zahraa El Maadi over a single 24 h period under hot summer conditions. Within the modeled conditions, scenarios with greater tree canopy generally produced lower pedestrian-level air temperatures, although the differences were small and varied by receptor and time of day. At 16:00 and 20:00, however, these reductions were no larger than those of the existing vegetation pattern (SC2). Water-containing scenarios tended to increase RH, and green roofs showed limited direct influence at street level. The response varied by receptor, and the maximum-NBS scenario was not uniformly the highest-performing

configuration among the tested scenarios, emphasizing the importance of local geometry and placement. Across the three pedestrian receptors and the reporting times of 12:00, 16:00, and 20:00, the simulated air-temperature reductions associated with the cooler NBS configurations were approximately 0.4–1.6 °C, depending on location and time of day. The upper value (approximately 1.6 °C at Receptor 1) occurred at 12:00, five hours after model initialization; when only the 16:00 and 20:00 outputs were considered, the maximum reduction was approximately 1.0 °C. This range refers to Ta only; PET was evaluated separately and remained high during the hottest hours.

A targeted one-at-a-time (OAT) sensitivity analysis of air-temperature forcing (±2 °C) and inflow wind speed (3.0 and 6.0 m/s) showed that the relative SC1–SC5 response depended on forcing condition, receptor location, and time of day. Across the four perturbed conditions, SC5 was cooler than SC1 in 21 of 36 receptor–time–condition comparisons (58.3%) and had lower PET in 20 of 36 comparisons (55.6%), indicating that the higher-tree-canopy configuration did not provide a uniform thermal advantage under all conditions. These NBS measures should also be integrated with built shading, appropriate surface materials, and ventilation-sensitive urban design to achieve greater thermal-comfort improvements. The complementary MyTree assessment illustrates the potential for tree planting to provide longer-term carbon, stormwater, and air-quality co-benefits beyond short-term microclimatic performance. However, because the Cairo location was not supported by MyTree and U.S. national averages were used for this run, the ecosystem-service outputs—particularly the stormwater estimates—should be regarded as illustrative rather than locally calibrated values for Cairo; MyTree monetary outputs were not used in the decision-matrix scoring. The main contribution of this study lies in connecting mobility-led green-space loss with site-specific NBS scenario assessment and an integrated planning framework for the case-study context. The framework links redevelopment-induced land-cover change, microclimatic simulation, ecosystem-service assessment, water-resource considerations, and planning priorities. The decision-matrix weighting analysis showed that SC5 ranked first under Equal Weighting, Water Balance Priority, and Tree Ecosystem Services Priority, whereas SC7 ranked first when Microclimate and Comfort were prioritized. This indicates that the preferred NBS configuration depends on the planning objective rather than on maximizing a single intervention. Overall, the study highlights that NBS should be applied as a context-sensitive planning strategy rather than through maximum greening alone. However, the findings are specific to the modeled site, scenarios, assumptions, meteorological forcing, and 24 h simulation period and should therefore be interpreted as comparative scenario-based evidence rather than site-calibrated predictions.

Supplementary Materials: The following supporting information can be downloaded at: https://www.mdpi.com/article/10.3390/architecture6040201/s1. Raw Data: Supplementary File S1: NBS decision-matrix workbook; Supplementary File S2: Summary baseline-relative comparison table and graphs for Ta, PET, RH, and WS; Supplementary File S3: Receptor-level ENVI-met outputs; Supplementary File S4: ENVI-met meteorological forcing/input file; Supplementary File S5: OAT sensitivity-analysis workbook with receptor-level Ta, RH, WS, and PET values. Interactive Findings Dashboard: Nature-based solutions on a widened Cairo Street—Interactive Dashboard.

Author Contributions: Conceptualization, A.E.Z. and W.M.E.-B.; methodology, A.E.Z., W.M.E.-B. and S.E.K.; software, A.E.Z.; validation, A.E.Z. and W.M.E.-B.; formal analysis, A.E.Z.; investigation, A.E.Z.; resources, A.E.Z.; data curation, A.E.Z.; writing—original draft preparation, A.E.Z.; writing—review and editing, S.E.K. and W.M.E.-B.; visualization, A.E.Z. All authors have read and agreed to the published version of the manuscript.

Funding: This research received no external funding.

Institutional Review Board Statement: Not applicable.

Informed Consent Statement: Not applicable.

Data Availability Statement: The data supporting the findings of this study are provided in the Supplementary Materials, including the NBS decision-matrix workbook (Supplementary File S1), the summary baseline-relative comparison table and summary graphs for Ta, PET, RH, and WS (Supplementary File S2), the receptor-level ENVI-met outputs used in the analysis (Supplementary File S3), the ENVI-met meteorological forcing/input file (Supplementary File S4), and the OAT sensitivity workbook with receptor-level Ta, RH, WS, and PET values and all corresponding calculations (Supplementary File S5).

Acknowledgments: During the preparation of this study, the authors used ChatGPT (OpenAI; GPT-5.6) to generate graphics illustrating overall scenario performance, PET values, and decision-matrix results, based on author-provided data and inputs for an interactive Excel workbook. The authors also used Claude (Anthropic; Claude Sonnet 5) for language proofreading, editorial refinement, and to generate the dashboard and the interactive relationships. ENVI-met simulation tool was provided by the Smart and Future Cities Laboratory for Sustainable Urban Solution (SFCL), a research laboratory in the Urban Design and Planning Department, Faculty of Engineering, Ain Shams University. The authors have reviewed and edited the output and take full responsibility for the content of this publication.

Conflicts of Interest: The authors declare no conflicts of interest. The funders had no role in the design of the study; in the collection, analysis, or interpretation of data; in the writing of the manuscript; or in the decision to publish the results.

Abbreviations

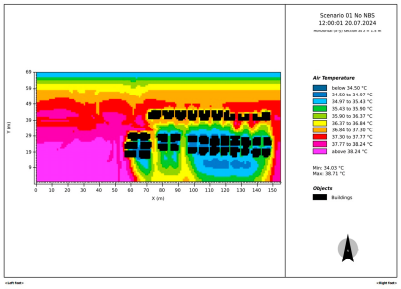
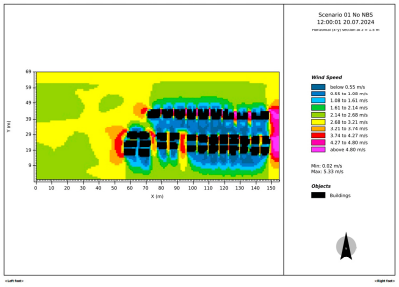
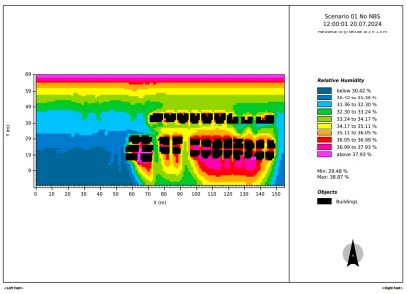
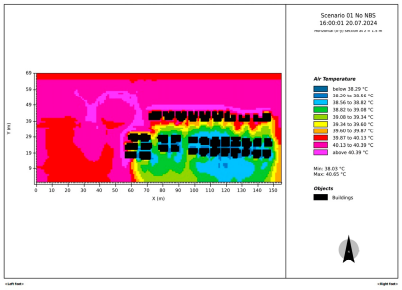
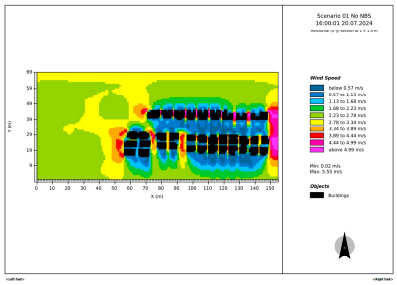
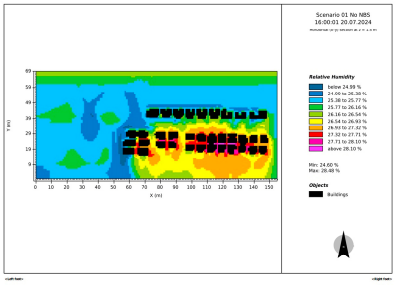
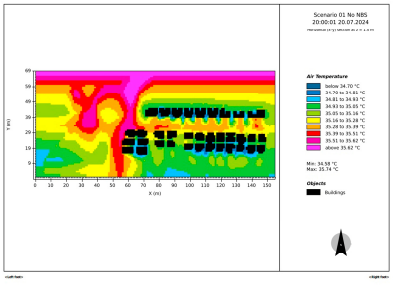
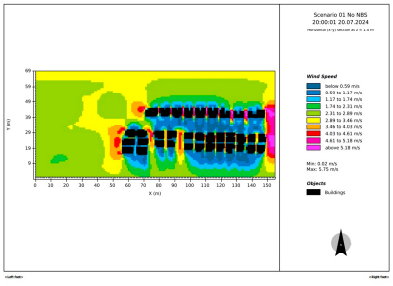
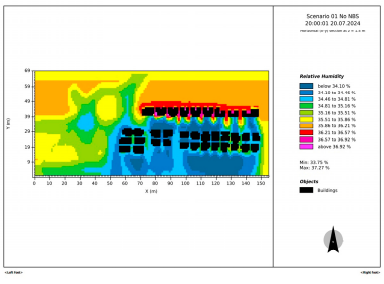
The following abbreviations are used in this manuscript:

NBS	Nature-Based Solution
ENVI-met	ENVI-met microclimate simulation model
T_a	Air Temperature
WS	Wind Speed
RH	Relative Humidity
PET	Physiological Equivalent Temperature
UHI	Urban Heat Island
IUCN	International Union for Conservation of Nature
i-Tree	i-Tree ecosystem-service assessment software
PMV	Predicted Mean Vote
PPD	Predicted Percentage Dissatisfied
UTCI	Universal Thermal Climate Index
SET	Standard Effective Temperature
EPW	EnergyPlus Weather file
SC	Scenario
R1/R2/R3	Receptor 1/Receptor 2/Receptor 3
CO_2	Carbon Dioxide
°C	Degrees Celsius
m/s	Meters per second
m^2	Square meters
h	Hour(s)
N	North
E	East
m	Meter
s	Second
DBH	Diameter at Breast Height
IA	Index of Agreement
R^2	Coefficient of Determination

BIO-met	ENVI-met BIO-met thermal-comfort module
USDA	United States Department of Agriculture
SFCL	Smart and Future Cities Laboratory
$PM_{2.5}$	Particulate Matter ≤ 2.5 µm
BWh	Hot Desert Climate (Köppen Climate Classification)
ML	Megaliter
L	Liter
kg	Kilogram
mm	Millimeter
cm	Centimeter
CFD	Computational Fluid Dynamics
USD	United States dollar
ES	Ecosystem services
OAT	One-at-a-time
pp	Percentage points

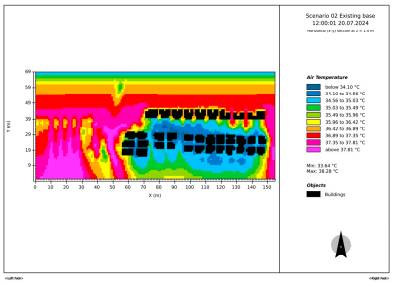
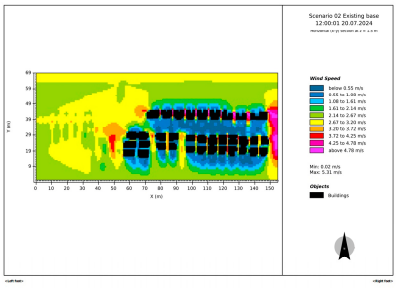
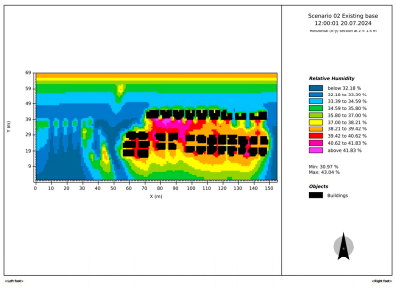
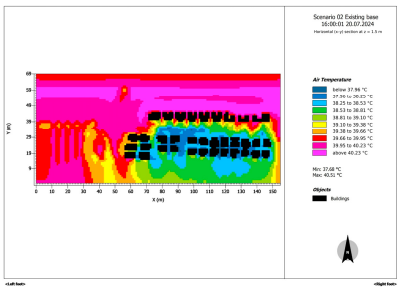
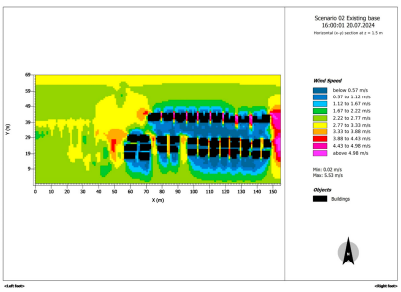
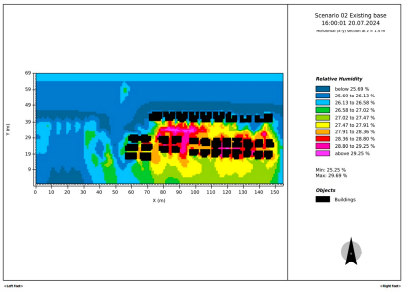
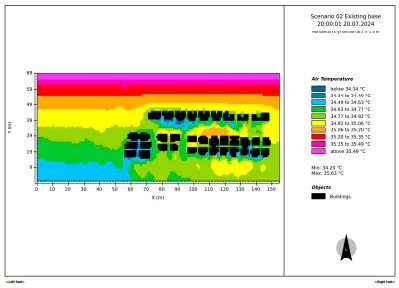
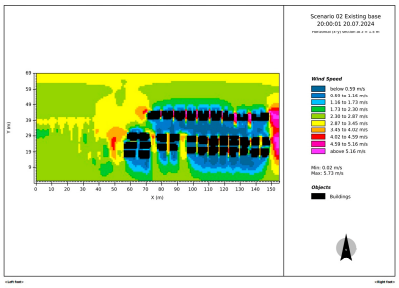
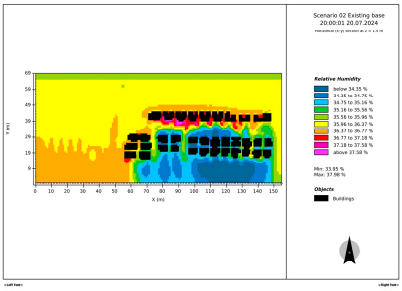
Appendix A

Table A1. SC1 (no vegetation).

At 12:00		
Air Temperature	**Wind Speed**	**Relative Humidity**
		
At 16:00		
		
At 20:00		
		

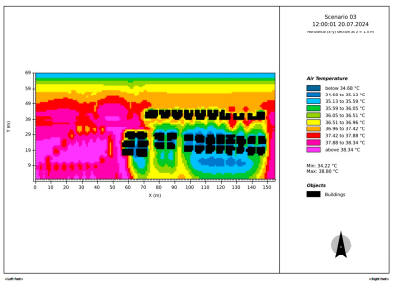
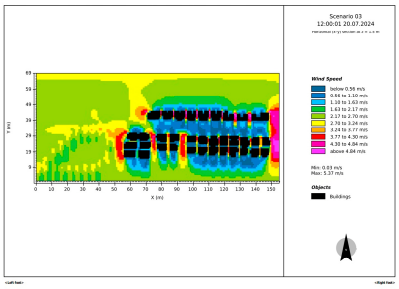
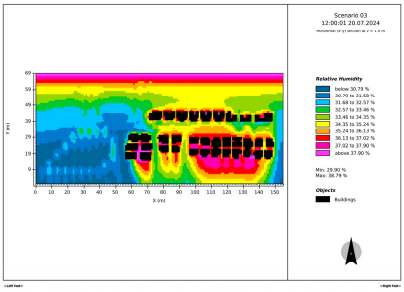
Appendix B

Table A2. SC2 (existing NBS).

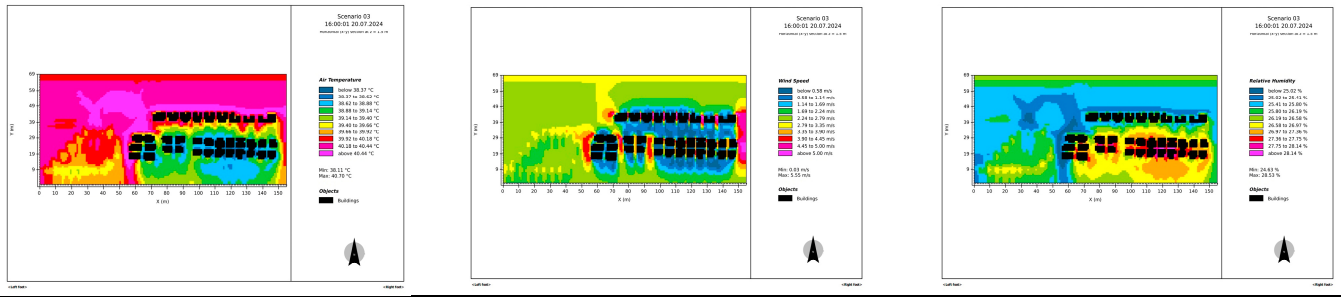
At 12:00		
Air Temperature	**Wind Speed**	**Relative Humidity**
		
At 16:00		
		
At 20:00		
		

Appendix C

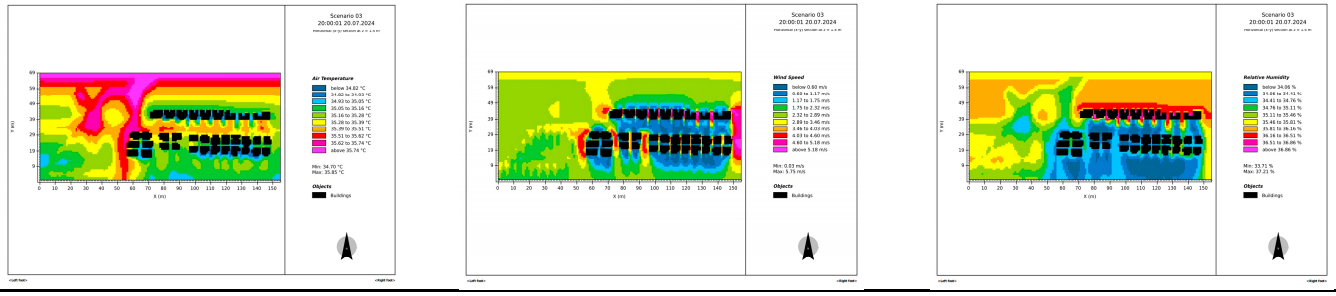
Table A3. SC3 (5% trees and 5% grass).

At 12:00		
Air Temperature	**Wind Speed**	**Relative Humidity**
		
At 16:00		

https://doi.org/10.3390/architecture6040201



At 20:00

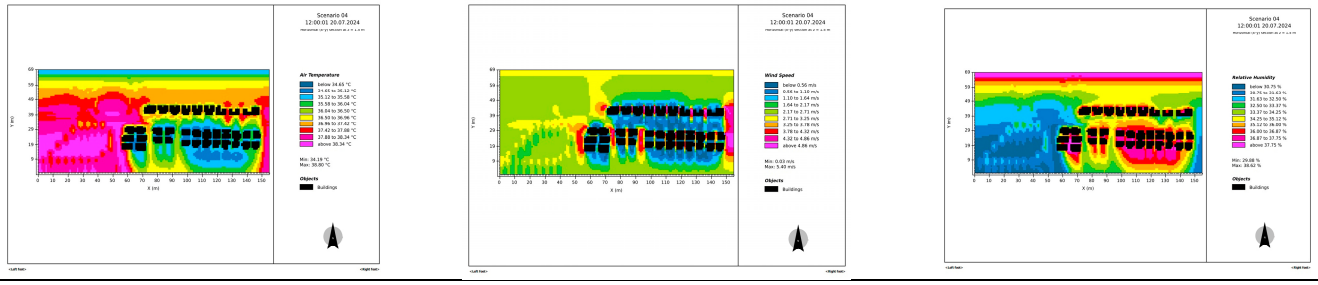


Appendix D

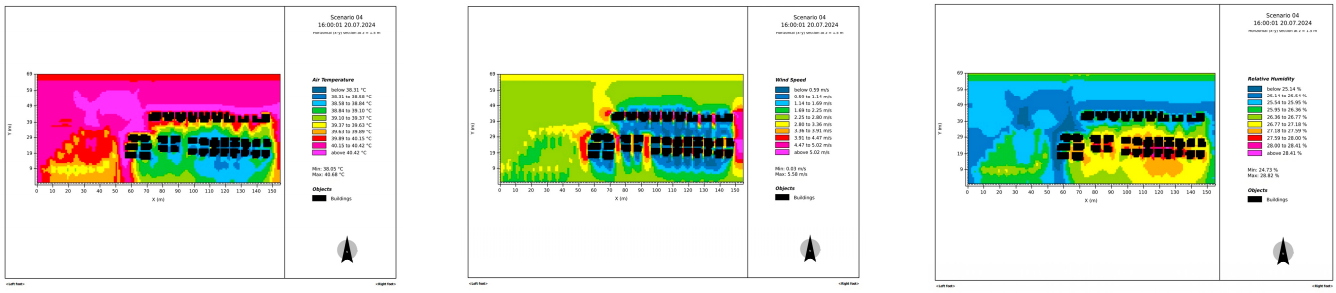
Table A4. SC4 (5% trees, 5% grass, and 5% green roof).

At 12:00

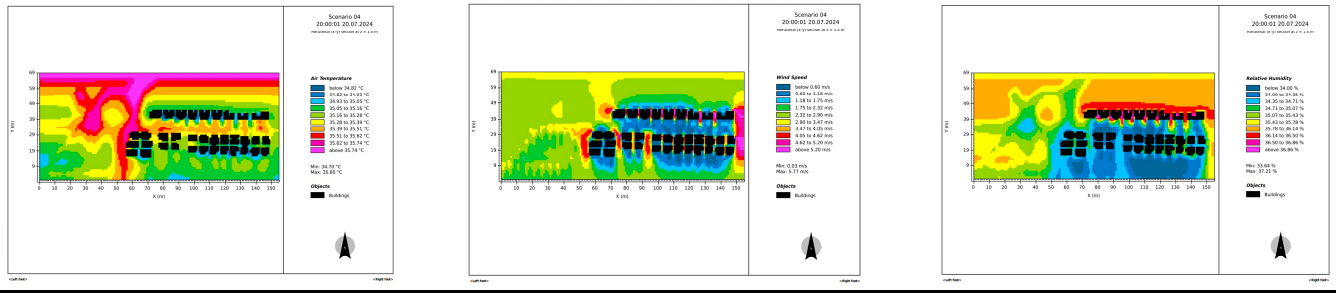
Air Temperature	Wind Speed	Relative Humidity



At 16:00



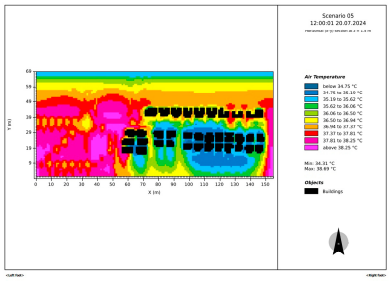
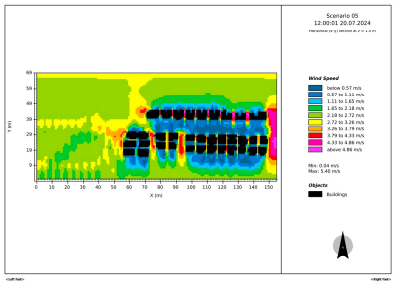
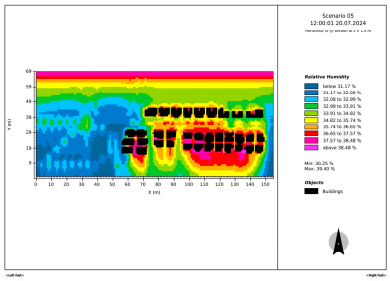
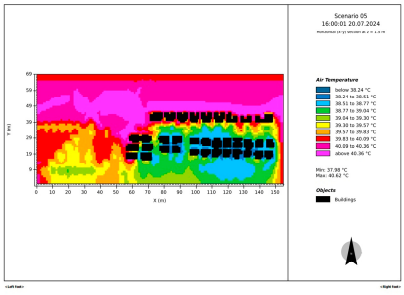
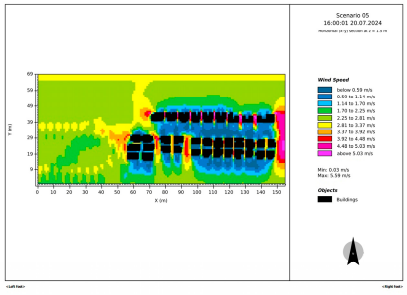
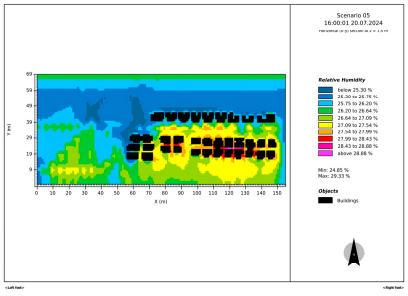
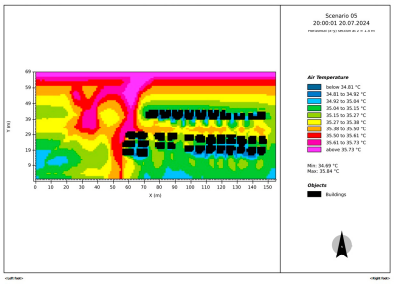
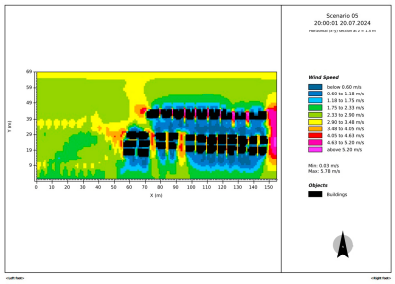
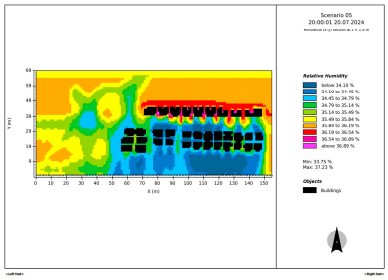
At 20:00



https://doi.org/10.3390/architecture6040201

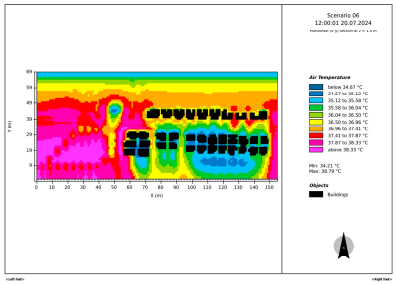
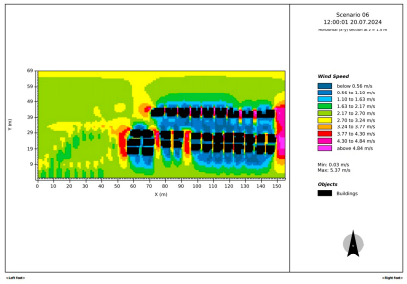
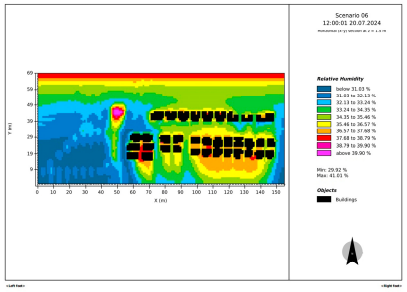
Appendix E

Table A5. SC5 (10% tree canopy and 5% grass).

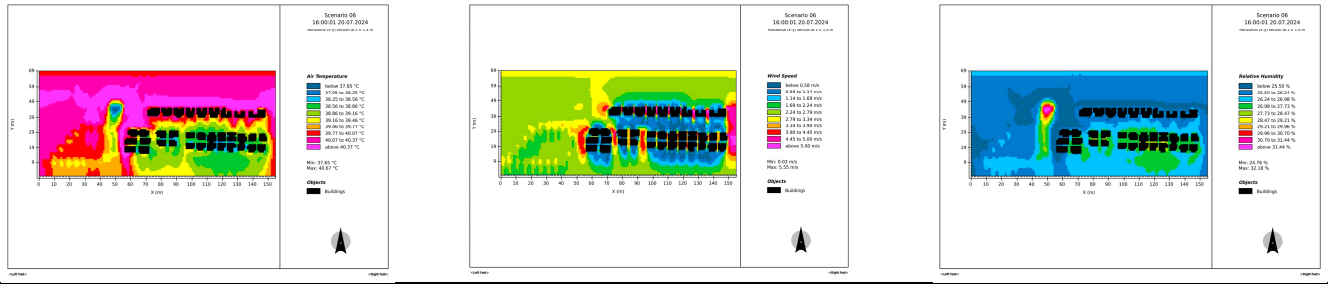
At 12:00		
Air Temperature	**Wind Speed**	**Relative Humidity**
		
At 16:00		
		
At 20:00		
		

Appendix F

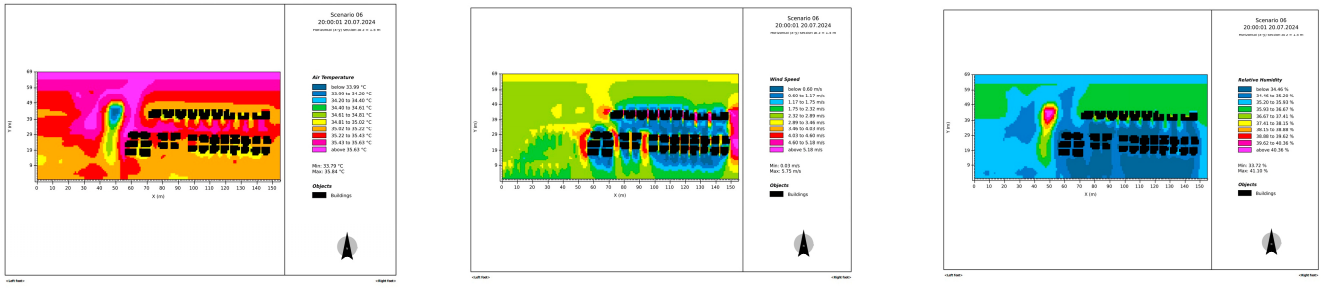
Table A6. SC6 (5% tree, 5% grass, and 5% water surface).

At 12:00		
Air Temperature	**Wind Speed**	**Relative Humidity**
		
At 16:00		

https://doi.org/10.3390/architecture6040201



At 20:00

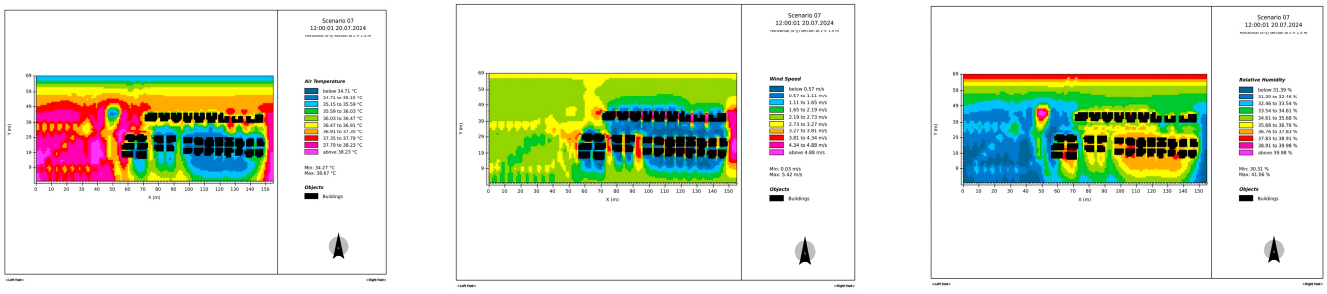


Appendix G

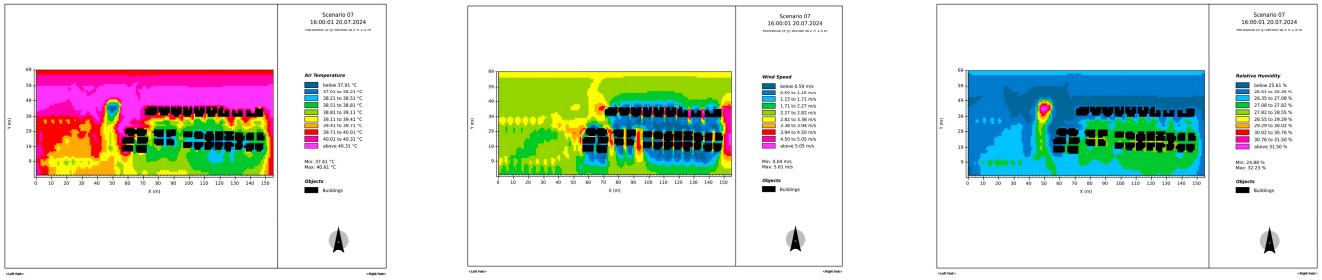
Table A7. SC7 (all elements: 10% trees, 5% green roof, 5% grass, and 5% water).

At 12:00

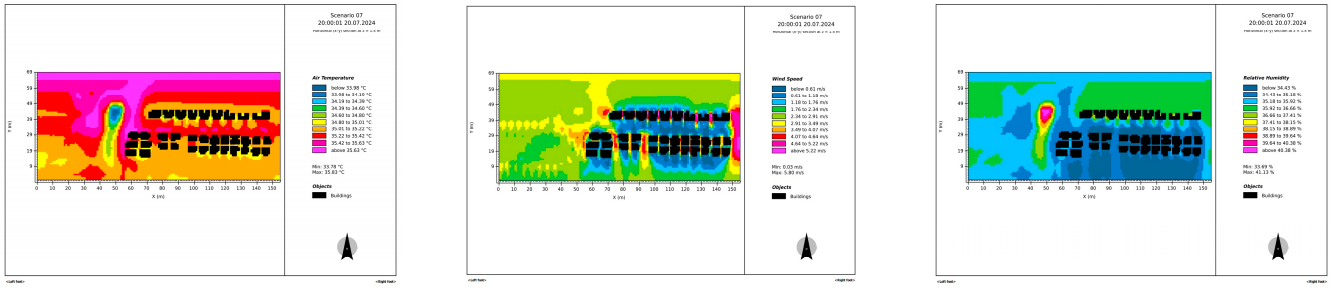
Air Temperature	Wind Speed	Relative Humidity



At 16:00



At 20:00



https://doi.org/10.3390/architecture6040201

References

1. Balbi, S.; Bagstad, K.J.; Magrach, A.; Sanz, M.J.; Aguilar-Amuchastegui, N.; Giupponi, C.; Villa, F. The global environmental agenda urgently needs a semantic web of knowledge. *Environ. Evid.* **2022**, *11*, 5. https://doi.org/10.1186/s13750-022-00258-y.
2. Shafaghat, A.; Manteghi, G.; Keyvanfar, A.; Bin Lamit, H.; Saito, K.; Ossen, D.R. Street geometry factors influence urban microclimate in tropical coastal cities: A review. *Environ. Clim. Technol.* **2016**, *17*, 61–75. https://doi.org/10.1515/rtuect-2016-0006.
3. Rugel, E.J.; Carpiano, R.M.; Henderson, S.B.; Brauer, M. Exposure to natural space, sense of community belonging, and adverse mental health outcomes across an urban region. *Environ. Res.* **2019**, *171*, 365–377. https://doi.org/10.1016/j.envres.2019.01.034.
4. Lotfata, A.; Cortesão, J.; Zinsmeister, H.; Steeneveld, G.; van Zeben, J.; Taylor, Z.; Tan, W.; Elkhateeb, S. Climate adaptation in informal areas in hot arid climates. *Sustain. Dev.* **2024**, *32*, 777–794. https://doi.org/10.1002/sd.2708.
5. European Commission. *Towards an EU Research and Innovation Policy Agenda for Nature-Based Solutions & Re-Naturing Cities*; Publications Office of the European Union: Luxembourg, 2015. https://doi.org/10.2777/765301.
6. Walters, G.; Cohen-Shacham, E.; Maginnis, S.; Lamarque, P. *Nature-Based Solutions to Address Global Societal Challenges*; (IUCN) International Union for Conservation of Nature: Gland, Switzerland, 2016. https://doi.org/10.2305/iucn.ch.2016.13.en.
7. Gunawardena, K.R.; Wells, M.J.; Kershaw, T. Utilising green and bluespace to mitigate urban heat island intensity. *Sci. Total Environ.* **2017**, *584–585*, 1040–1055. https://doi.org/10.1016/j.scitotenv.2017.01.158.
8. Kaçmaz Akkurt, G.; Şemsiyeci, S. Evaluation of Nature-Based Solutions to Improve the Urban Microclimate in Mediterranean Climate Conditions: A Case Study of Izmir-Karsıyaka. *Sustainability* **2024**, *16*, 2646. https://doi.org/10.3390/su16072646.
9. Badawi, A.; Galal Ahmed, K. Sponge city in hot-arid regions: Review of potential and challenges for application. *Front. Sustain. Cities* **2026**, *8*, 1779222. https://doi.org/10.3389/frsc.2026.1779222.
10. Meerow, S.; Natarajan, M.; Krantz, D. Green infrastructure performance in arid and semi-arid urban environments. *Urban Water J.* **2021**, *18*, 275–285. https://doi.org/10.1080/1573062X.2021.1877741.
11. Soltanifard, H.; Amani-Beni, M. The cooling effect of urban green spaces as nature-based solutions for mitigating urban heat: Insights from a decade-long systematic review. *Clim. Risk Manag.* **2025**, *49*, 100731. https://doi.org/10.1016/j.crm.2025.100731.
12. Elnabawi, M.H.; Hamza, N.; Ahmed, T.M.F.; Santamouris, M. Integrated passive cooling strategies for neighborhood-scale urban heat mitigation in a hot-arid city: ENVI-met simulations in Al Ain, UAE. *Results Eng.* **2026**, *29*, 109840. https://doi.org/10.1016/j.rineng.2026.109840.
13. Al-Hagla, K.; Alrawaf, T.I. Operationalizing Nature-Based Solutions for Urban Sustainability in Hyper-Arid Regions: The Case of the Eastern Province, Saudi Arabia. *Sustainability* **2025**, *17*, 8036. https://doi.org/10.3390/su17178036.
14. Elbardisy, W.M.; Salheen, M.A.; Fahmy, M. Solar irradiance reduction using optimized green infrastructure in arid hot regions: A case study in El-Nozha District, Cairo, Egypt. *Sustainability* **2021**, *13*, 9617. https://doi.org/10.3390/su13179617.
15. Abedrabboh, O.; Fountoukis, C.; Al-Ansari, T.; Alfarra, M.R. Simulating microclimate adaptation: Evaluating heat mitigation strategies for Doha, Qatar, under current and future climate conditions. *Sustain. Cities Soc.* **2025**, *132*, 106777. https://doi.org/10.1016/j.scs.2025.106777.
16. IQAir. Air Quality Map. Available online: https://www.iqair.com/air-quality-map (accessed on 4 April 2025).
17. Tominaga, Y.; Blocken, B. Wind tunnel analysis of flow and dispersion in cross-ventilated isolated buildings: Impact of opening positions. *J. Wind Eng. Ind. Aerodyn.* **2016**, *155*, 74–88. https://doi.org/10.1016/j.jweia.2016.05.007.
18. Blocken, B. Computational Fluid Dynamics for urban physics: Importance, scales, possibilities, limitations and ten tips and tricks towards accurate and reliable simulations. *Build. Environ.* **2015**, *91*, 219–245. https://doi.org/10.1016/j.buildenv.2015.02.015.
19. Maronga, B.; Gryschka, M.; Heinze, R.; Hoffmann, F.; Kanani-Sühring, F.; Keck, M.; Ketelsen, K.; Letzel, M.O.; Sühring, M.; Raasch, S. The Parallelized Large-Eddy Simulation Model (PALM) version 4.0 for atmospheric and oceanic flows: Model formulation, recent developments, and future perspectives. *Geosci. Model Dev.* **2015**, *8*, 2515–2544. https://doi.org/10.5194/gmd-8-2515-2015.
20. Matzarakis, A.; Rutz, F.; Mayer, H. Modelling radiation fluxes in simple and complex environments—Application of the RayMan model. *Int. J. Biometeorol.* **2007**, *51*, 323–334. https://doi.org/10.1007/s00484-006-0061-8.
21. Lindberg, F.; Holmer, B.; Thorsson, S. SOLWEIG 1.0—Modelling spatial variations of 3D radiant fluxes and mean radiant temperature in complex urban settings. *Int. J. Biometeorol.* **2008**, *52*, 697–713. https://doi.org/10.1007/s00484-008-0162-7.
22. Tsoka, S.; Tsikaloudaki, A.; Theodosiou, T. Analyzing the ENVI-met microclimate model's performance and assessing cool materials and urban vegetation applications—A review. *Sustain. Cities Soc.* **2018**, *43*, 55–76. https://doi.org/10.1016/j.scs.2018.08.009.
23. Detommaso, M.; Costanzo, V.; Nocera, F. Application of weather data morphing for calibration of urban ENVI-met microclimate models. Results and critical issues. *Urban Clim.* **2021**, *38*, 100895. https://doi.org/10.1016/j.uclim.2021.100895.

24. ENVI-Met. ENVI-Met—Decode Urban Nature with ENVI-Met Software. Available online: https://www.envi-met.com/ (accessed on 1 June 2025).
25. EnergyPlus. Weather Data by Location. Available online: https://energyplus.net/weather-location/africa_wmo_region_1/EGY//EGY_Cairo.623660_IWEC (accessed on 28 July 2025).
26. Elbardisy, W.M.; Salheen, M.A.; Fahmy, M. The Impact of Street Trees on a Typical Urban Canyon in Eastern Cairo Region. *IOP Conf. Ser. Earth Environ. Sci.* **2022**, *1056*, 012025. https://doi.org/10.1088/1755-1315/1056/1/012025.
27. Mosisa, G.B.; Bedadi, B.; Dalle, G.; Tassie, N. Nature-based solutions for urban climate resilience: Implementation, contribution, and effectiveness. *Nat.-Based Solut.* **2025**, *8*, 100245. https://doi.org/10.1016/j.nbsj.2025.100245.
28. Benlahbib, F.Z.; Alkama, D.; Mohamed, N.H.; Harrat, Z.R.; Bennaceur, S.; Işık, E.; Avcil, F.; Hilal, N.; Hama, S.M.; Hadzima-Nyarko, M. Impact of Urban Morphology on Microclimate and Thermal Comfort in Arid Cities: A Comparative Study and Modeling in Béchar. *Sustainability* **2026**, *18*, 659. https://doi.org/10.3390/su18020659.
29. Verma, D.; Mumm, O.; Carlow, V.M. CoolPaths: Street-scale Physiological Equivalent Temperature (PET) mapping and cooler-routes planning using open data. *City Environ. Interact.* **2026**, *30*, 100349. https://doi.org/10.1016/j.cacint.2026.100349.
30. i-Tree. Available online: https://www.itreetools.org/ (accessed on 28 September 2025).
31. Meteonorm. Meteonorm Version 8—Meteonorm (en). Available online: https://meteonorm.com/en/meteonorm-version-8 (accessed on 12 April 2025).
32. Gomaa, M.M.; El Menshawy, A.; Nabil, J.; Ragab, A. Investigating the Impact of Various Vegetation Scenarios on Outdoor Thermal Comfort in Low-Density Residential Areas of Hot Arid Regions. *Sustainability* **2024**, *16*, 3995. https://doi.org/10.3390/su16103995.
33. Ayyad, Y.N.; Sharples, S. ENVI-met validation and sensitivity analysis using field measurements in a hot arid climate. In *IOP Conference Series: Earth and Environmental Science*; Institute of Physics Publishing: Bristol, UK, 2019. https://doi.org/10.1088/1755-1315/329/1/012040.
34. Elkhateeb, S.; Anwar, R. Parametric Optimization of Urban Street Tree Placement: Computational Workflow for Dynamic Shade Provision in Hot Climates. *Urban Sci.* **2025**, *9*, 504. https://doi.org/10.3390/urbansci9120504.
35. Abdo, A.; Othman, A.M.; Ahmed, D. Greywater recycling and solar photovoltaic integration for sustainable water and energy management in urban Egypt. *Sci. Rep.* **2026**, *16*, 14389. https://doi.org/10.1038/s41598-026-49932-y.
36. Murakami, M.; UNU. *Managing Water for Peace in the Middle East*; United Nations University Press: Tokyo, Japan, 1995.
37. Shammas, N.K. Investigation of Irrigation Water Application Rates to Landscaped Areas in Riyadh. *J. King Saud Univ. Eng. Sci.* **1991**, *3*, 147–164. https://doi.org/10.1016/S1018-3639(18)30543-9.
38. Schweitzer, O.; Erell, E. Evaluation of the energy performance and irrigation requirements of extensive green roofs in a water-scarce Mediterranean climate. *Energy Build.* **2014**, *68*, 25–32. https://doi.org/10.1016/j.enbuild.2013.09.012.
39. Santamouris, M. Cooling the cities—A review of reflective and green roof mitigation technologies to fight heat island and improve comfort in urban environments. *Sol. Energy* **2014**, *103*, 682–703. https://doi.org/10.1016/j.solener.2012.07.003.
40. Oke, T.R.; Mills, G.; Christen, A.; Voogt, J.A. *Urban Climates*; Cambridge University Press: Cambridge, UK, 2017. https://doi.org/10.1017/9781139016476.
41. Bowler, D.E.; Buyung-Ali, L.; Knight, T.M.; Pullin, A.S. Urban greening to cool towns and cities: A systematic review of the empirical evidence. *Landsc. Urban Plan.* **2010**, *97*, 147–155. https://doi.org/10.1016/j.landurbplan.2010.05.006.
42. Wei, R.; Yan, J.; Cui, Y.; Song, D.; Yin, X.; Sun, N. Studies on the Specificity of Outdoor Thermal Comfort during the Warm Season in High-Density Urban Areas. *Buildings* **2023**, *13*, 2473. https://doi.org/10.3390/buildings13102473.
43. Akbari, H.; Pomerantz, M.; Taha, H. Cool Surfaces and shade trees to reduce energy use and improve air quality in urban areas. *Sol. Energy* **2001**, *70*, 295–310. https://doi.org/10.1016/S0038-092X(00)00089-X.
44. Rahman, M.A.; Moser, A.; Gold, A.; Rötzer, T.; Pauleit, S. Vertical air temperature gradients under the shade of two contrasting urban tree species during different types of summer days. *Sci. Total Environ.* **2018**, *633*, 100–111. https://doi.org/10.1016/j.scitotenv.2018.03.168.
45. Taleghani, M.; Kleerekoper, L.; Tenpierik, M.; Van Den Dobbelsteen, A. Outdoor thermal comfort within five different urban forms in the Netherlands. *Build. Environ.* **2015**, *83*, 65–78. https://doi.org/10.1016/j.buildenv.2014.03.014.
46. Van de Walle, A.; Kim, M.; Alam, K.; Wang, X.; Wu, D.; Dash, S.R.; Rabaey, K.; Kim, J. Greywater reuse as a key enabler for improving urban wastewater management. *Environ. Sci. Ecotechnol.* **2023**, *16*, 100277. https://doi.org/10.1016/j.ese.2023.100277.

Disclaimer/Publisher's Note: The statements, opinions and data contained in all publications are solely those of the individual author(s) and contributor(s) and not of MDPI and/or the editor(s). MDPI and/or the editor(s) disclaim responsibility for any injury to people or property resulting from any ideas, methods, instructions or products referred to in the content.